INTERNATIONAL JOURNAL FOR NUMERICAL METHODS IN ENGINEERING
Int. J. Numer. Meth. Engng 2007; **69**:114–161
Published online 5 June 2006 in Wiley InterScience (www.interscience.wiley.com). DOI: 10.1002/nme.1759

Finite element response sensitivity analysis using three-field mixed formulation: General theory and application to frame structures

M. Barbato[1,‡,¶], A. Zona[1,2,§,‖] and J. P. Conte[1,*,†,**]

[1]*Department of Structural Engineering, University of California at San Diego, 9500 Gilman Drive, La Jolla, CA 92093-0085, U.S.A.*
[2]*Department PROCAM, University of Camerino, Viale della Rimembranza, Ascoli Piceno 63100, Italy*

SUMMARY

This paper presents a method to compute response sensitivities of finite element models of structures based on a three-field mixed formulation. The methodology is based on the direct differentiation method (DDM), and produces the response sensitivities consistent with the numerical finite element response. The general formulation is specialized to frame finite elements and details related to a newly developed steel–concrete composite frame element are provided. DDM sensitivity results are validated through the forward finite difference method (FDM) using a finite element model of a realistic steel–concrete composite frame subjected to quasi-static and dynamic loading. The finite element model of the structure considered is constructed using both monolithic frame elements and composite frame elements with deformable shear connection based on the three-field mixed formulation. The addition of the analytical sensitivity computation algorithm presented in this paper extends the use of finite elements based on a three-field mixed formulation to applications that require finite element response sensitivities. Such applications include structural reliability analysis, structural optimization, structural identification, and finite element model updating. Copyright © 2006 John Wiley & Sons, Ltd.

Received 16 December 2005; Accepted 14 March 2006

KEY WORDS: Hu–Washizu functional; three-field mixed finite element formulation; material constitutive parameters; finite element response sensitivity; steel–concrete composite beam

*Correspondence to: J. P. Conte, Department of Structural Engineering, University of California at San Diego, 9500 Gilman Drive, La Jolla, CA 92093-0085, U.S.A.
†E-mail: jpconte@ucsd.edu
‡E-mail: mbarbato@ucsd.edu
§E-mail: azona@ucsd.edu, alessandro.zona@unicam.it
¶Graduate Student.
‖Assistant Professor and formerly Postgraduate Researcher.
**Professor.

Contract/grant sponsor: National Science Foundation; contract/grant number: CMS-0010112
Contract/grant sponsor: Pacific Earthquake Engineering Research (PEER) Center; contract/grant number: EEC-9701568

Copyright © 2006 John Wiley & Sons, Ltd.

1. INTRODUCTION

Finite element response sensitivities represent an essential ingredient for gradient-based optimization methods used to solve problems in structural optimization, structural reliability analysis, structural identification and finite element model updating [1, 2]. Finite element response sensitivities are also invaluable for gaining deeper insight into the effects and relative importance of the various geometric, material, and loading parameters defining the structure and its loading environment.

Sensitivity analysis formulations have been developed for displacement-based finite element models [3–5] and, recently, for force-based frame elements [6, 7]. The advantages gained in response analysis by using finite element formulations more advanced than the classical displacement-based formulation can be further extended to the realm of response sensitivity analysis [8].

A large body of research has been devoted to mixed finite element formulations since they were first introduced in the pioneering work of Pian [9]. Several finite elements based on different variational principles have been developed [10–14] and relationships among them have been established [15, 16]. Accuracy and performance have been thoroughly analysed and improved and important properties have been recognized and explained, such as equivalence between various stress recovery techniques [17] and ability to eliminate shear-locking effects for specific applications [14]. After more than three decades of research in the field, mixed finite elements are well established and largely adopted tools in a wide range of structural mechanics applications. However, to the authors knowledge, attempts of extending mixed finite element formulations to response sensitivity analysis by using the direct differentiation method (DDM) are limited to linear elastic and quasi-static analysis [18].

Multi-field mixed finite element formulations were proposed, among others, for finite elements widely used in the structural engineering community such as frame elements. Mixed frame elements are more accurate in nonlinear analysis than displacement-based elements and are a possible alternative to the recently established force-based elements [19]. Examples are available in the recent literature for monolithic beams [19–21] and for composite beams with deformable shear connection [22, 23].

This paper focuses on the formulation of finite element response sensitivity analysis in the case of a nonlinear three-field mixed approach derived from the Hu–Washizu variational principle, considering both quasi-static and dynamic loadings. The formulation presented here is based on the general DDM, which consists of differentiating consistently the space (finite element) and time (finite difference) discrete equations governing the structural response [4, 5]. The general formulation for finite element response sensitivity analysis using the three-field mixed formulation is then specialized and applied to frame finite element models. The results of the DDM are validated through the forward finite difference method (FDM) using as application example a realistic steel–concrete composite frame structure subjected to quasi-static and dynamic loading, respectively. Both monolithic frame elements [21] and composite frame elements with deformable shear connection [23] based on the three-field mixed formulation are included in this application example.

Copyright © 2006 John Wiley & Sons, Ltd.

DOI: 10.1002/nme

2. FINITE ELEMENT RESPONSE SENSITIVITY ANALYSIS

The computation of finite element response sensitivities to geometric, material and loading parameters requires extension of the finite element algorithms for response computation only. If r denotes a generic scalar response quantity, the sensitivity of r with respect to the geometric, material or loading parameter θ is expressed, by definition, as the (absolute) partial derivative of r with respect to the variable θ evaluated at $\theta = \theta_0$ i.e. $\partial r/\partial\theta|_{\theta=\theta_0}$ where θ_0 denotes the nominal value taken by the sensitivity parameter θ for the finite element response analysis.

In the sequel, the notation proposed by Kleiber *et al.* [2] is adopted and the case of a single sensitivity parameter is considered without loss of generality. Thus, the quantity $\mathrm{d}r/\mathrm{d}\theta$, called 'unconditional sensitivity' or 'unconditional derivative' of r with respect to θ, denotes the absolute partial derivative of the argument r with respect to the scalar variable θ (i.e. the derivative of response variable r with respect to the parameter θ considering both explicit and implicit dependencies). On the other hand, $\partial r/\partial\theta|_{\mathbf{z}}$, called 'conditional sensitivity' or 'conditional derivative' of r with respect to θ for $\mathbf{z}$ fixed, is defined as the partial derivative for r with respect to parameter θ when the vector of variables $\mathbf{z}$ is kept fixed.

It is assumed herein that the structural response is computed using a general-purpose nonlinear finite element analysis program based on the direct stiffness method, employing suitable numerical integration schemes at both the structure and element level. At each time step, after convergence of the incremental-iterative response computation, the consistent response sensitivities are calculated. According to the DDM (see References [3–8]), this requires the analytical differentiation of the finite element numerical scheme for response computation with respect to the sensitivity parameter θ in order to obtain the 'exact' or 'consistent' sensitivities of the computationally simulated system response. After spatial discretization using the finite element method, the equations of motion of a structural system, accounting for both material and geometric nonlinearities, take the form of the following nonlinear matrix differential equation:

$$\mathbf{M}(\theta)\ddot{\mathbf{u}}(t,\theta) + \mathbf{C}(\theta)\dot{\mathbf{u}}(t,\theta) + \mathbf{R}(\mathbf{u}(t,\theta),\theta) = \mathbf{F}(t,\theta) \tag{1}$$

where t is the time, θ the scalar sensitivity parameter (geometric, material or loading variable), $\mathbf{u}(t,\theta)$ the vector of nodal displacements, $\mathbf{M}(\theta)$ the mass matrix, $\mathbf{C}(\theta)$ the damping matrix, $\mathbf{R}(\mathbf{u}(t,\theta),\theta)$ the history-dependent internal (inelastic) resisting force vector, $\mathbf{F}(t,\theta)$ the applied dynamic load vector, and a superposed dot denotes one differentiation with respect to time.

We assume without loss of generality that the time continuous-spatially discrete equation of motion, Equation (1), is integrated numerically in time using a single-step time stepping scheme expressing the nodal acceleration vector $\ddot{\mathbf{u}}$ and nodal velocity vector $\dot{\mathbf{u}}$ at time t_{n+1} in terms of the nodal displacement vector $\mathbf{u}$ at time t_{n+1} and the nodal acceleration, velocity and displacement vectors at the previous time step t_n as

$$\ddot{\mathbf{u}}_{n+1} = a_1\mathbf{u}_{n+1} + a_2\mathbf{u}_n + a_3\dot{\mathbf{u}}_n + a_4\ddot{\mathbf{u}}_n \tag{2}$$

$$\dot{\mathbf{u}}_{n+1} = a_5\mathbf{u}_{n+1} + a_6\mathbf{u}_n + a_7\dot{\mathbf{u}}_n + a_8\ddot{\mathbf{u}}_n \tag{3}$$

Copyright © 2006 John Wiley & Sons, Ltd.

DOI: 10.1002/nme

Substituting Equations (2) and (3) in Equation (1) expressed at time t_{n+1} yields the following nonlinear matrix algebraic equation in the unknown $\mathbf{u}_{n+1} = \mathbf{u}(t_{n+1})$:

$$\tilde{\mathbf{F}}_{n+1} - [a_1\mathbf{M}\mathbf{u}_{n+1} + a_5\mathbf{C}\mathbf{u}_{n+1} + \mathbf{R}(\mathbf{u}_{n+1})] = \mathbf{0} \tag{4}$$

where

$$\tilde{\mathbf{F}}_{n+1} = \mathbf{F}_{n+1} - \mathbf{M}[a_2\mathbf{u}_n + a_3\dot{\mathbf{u}}_n + a_4\ddot{\mathbf{u}}_n] - \mathbf{C}[a_6\mathbf{u}_n + a_7\dot{\mathbf{u}}_n + a_8\ddot{\mathbf{u}}_n] \tag{5}$$

and a_i $(i = 1, \ldots, 8)$ denote the coefficients of the time stepping scheme. This formulation represents a general class of one-step implicit integration algorithms, containing the well-known Newmark-β and Wilson methods (see References [3–8]). In the case of the Newmark-β method [24], the integration coefficients are given by

$$a_1 = \frac{1}{(\Delta t)^2\beta_2}, \quad a_2 = -a_1, \quad a_3 = -\frac{1}{(\Delta t)\beta_2}, \quad a_4 = 1 - \frac{1}{2\beta_2}$$

$$a_5 = \frac{\beta_1}{(\Delta t)\beta_2}, \quad a_6 = -a_5, \quad a_7 = 1 - \frac{\beta_1}{\beta_2}, \quad a_8 = \left(1 - \frac{\beta_1}{2\beta_2}\right)(\Delta t)$$

where β_1 and β_2 are two parameters controlling the accuracy and stability of the numerical scheme (e.g. $\beta_1 = \frac{1}{2}$ and $\beta_2 = \frac{1}{4}$ for the unconditionally stable average acceleration method). Equation (4) represents the set of nonlinear algebraic equations for the unknown response quantities $\mathbf{u}_{n+1}$ that has to be solved at each time step $[t_n, t_{n+1}]$. In general, the subscript $(\ldots)_{n+1}$ indicates that the quantity to which it is attached is evaluated at discrete time t_{n+1}.

We assume that $\mathbf{u}_{n+1}$ is the converged solution (up to some iteration residuals satisfying a specified tolerance usually taken in the vicinity of the machine precision) for the current time step $[t_n, t_{n+1}]$. Then, we differentiate Equation (4) with respect to θ using the chain rule of differentiation and recognizing that $\mathbf{R}(\mathbf{u}_{n+1}) = \mathbf{R}(\mathbf{u}_{n+1}(\theta), \theta)$ (i.e. the structure inelastic resisting force vector depends on θ both implicitly, through $\mathbf{u}_{n+1}$, and explicitly), which yields the following response sensitivity equation at the structure level (see References [3–5]):

$$\begin{aligned}&[a_1\mathbf{M} + a_5\mathbf{C} + (\mathbf{K}_T^{\text{stat}})_{n+1}]\frac{\mathrm{d}\mathbf{u}_{n+1}}{\mathrm{d}\theta}\\ &\quad = \frac{\mathrm{d}\tilde{\mathbf{F}}_{n+1}}{\mathrm{d}\theta} - \left(a_1\frac{\mathrm{d}\mathbf{M}}{\mathrm{d}\theta} + a_5\frac{\mathrm{d}\mathbf{C}}{\mathrm{d}\theta}\right)\mathbf{u}_{n+1} - \left.\frac{\partial\mathbf{R}(\mathbf{u}_{n+1}(\theta), \theta)}{\partial\theta}\right|_{\mathbf{u}_{n+1}}\end{aligned} \tag{6}$$

where

$$\begin{aligned}\frac{\mathrm{d}\tilde{\mathbf{F}}_{n+1}}{\mathrm{d}\theta} &= \frac{\mathrm{d}\mathbf{F}_{n+1}}{\mathrm{d}\theta} - \frac{\mathrm{d}\mathbf{M}}{\mathrm{d}\theta}(a_2\mathbf{u}_n + a_3\dot{\mathbf{u}}_n + a_4\ddot{\mathbf{u}}_n) - \mathbf{M}\left[a_2\frac{\mathrm{d}\mathbf{u}_n}{\mathrm{d}\theta} + a_3\frac{\mathrm{d}\dot{\mathbf{u}}_n}{\mathrm{d}\theta} + a_4\frac{\mathrm{d}\ddot{\mathbf{u}}_n}{\mathrm{d}\theta}\right]\\ &\quad - \frac{\mathrm{d}\mathbf{C}}{\mathrm{d}\theta}[a_6\mathbf{u}_n + a_7\dot{\mathbf{u}}_n + a_8\ddot{\mathbf{u}}_n] - \mathbf{C}\left[a_6\frac{\mathrm{d}\mathbf{u}_n}{\mathrm{d}\theta} + a_7\frac{\mathrm{d}\dot{\mathbf{u}}_n}{\mathrm{d}\theta} + a_8\frac{\mathrm{d}\ddot{\mathbf{u}}_n}{\mathrm{d}\theta}\right]\end{aligned} \tag{7}$$

Copyright © 2006 John Wiley & Sons, Ltd.

DOI: 10.1002/nme

The term $(\mathbf{K}_T^{\text{stat}})_{n+1}$ in Equation (6) denotes the static consistent (or algorithmic) tangent stiffness matrix of the structure at time t_{n+1}. The last term on the RHS of Equation (6) represents the partial derivative with respect to θ of the internal resisting force vector, $\mathbf{R}(\mathbf{u}_{n+1})$, under the condition that the displacement vector $\mathbf{u}_{n+1}$ remains fixed, and is computed through direct stiffness assembly of the element resisting force derivatives for fixed element nodal displacements.

The above formulation, expressed for the case of dynamic loading, contains the quasi-static load case as a particular case, obtained by simply equating to zero in Equations (4)–(7) all terms containing the mass and damping matrices as well as their derivatives with respect to θ.

3. RESPONSE SENSITIVITY ANALYSIS AT THE ELEMENT LEVEL

3.1. General geometric and material nonlinear theory including shape sensitivity

The general formulation is presented for a structural model including geometric and material nonlinearities and considering material, shape, and loading sensitivities. An isoparametric finite element in total Lagrangian formulation is considered.

Following Reference [14], three different domains need to be introduced:

(a) the parent domain, denoted by the symbol $\square$, with element coordinates $\boldsymbol{\xi} = [\xi_1, \xi_2, \xi_3]^{\mathrm{T}}$;
(b) the reference (or initial configuration) domain, Ω_0, with coordinates $\mathbf{X} = [X_1, X_2, X_3]^{\mathrm{T}}$;
(c) the current configuration domain, $\Omega(t)$, with coordinates $\mathbf{x}(t)=[x_1(t), x_2(t), x_3(t)]^{\mathrm{T}}$, where t denotes time (or pseudo-time in quasi-static analysis).

Correspondingly, the following one-to-one mappings are defined:

(a) from parent domain to current configuration: $\mathbf{x} = \mathbf{x}(\boldsymbol{\xi}, t)$;
(b) from parent domain to reference configuration: $\mathbf{X} = \mathbf{X}(\boldsymbol{\xi})$;
(c) from reference configuration to current configuration: $\mathbf{x} = \mathbf{x}(\mathbf{X}, t)$.

It is supposed that the above mappings satisfy certain conditions of regularity such that the inverse mappings exist and the motion is well defined and sufficiently smooth.

As measure of strain, the Green–Lagrange strain is adopted, defined in tensorial form using the index notation as

$$E_{ij}^{\mathrm{G}} = \frac{1}{2}\left(\frac{\partial u_i}{\partial X_j} + \frac{\partial u_j}{\partial X_i} + \frac{\partial u_k}{\partial X_i}\frac{\partial u_k}{\partial X_j}\right), \quad i, j = 1, 2, 3 \tag{8}$$

Using Voigt notation, the vector form of the Green–Lagrange strain tensor is defined as

$$\mathbf{E}_{\mathrm{G}} = [E_{11}^{\mathrm{G}}, E_{22}^{\mathrm{G}}, E_{33}^{\mathrm{G}}, 2E_{23}^{\mathrm{G}}, 2E_{13}^{\mathrm{G}}, 2E_{12}^{\mathrm{G}}]^{\mathrm{T}} \tag{9}$$

The work conjugate stress measure of the Green–Lagrange strain tensor is the second Piola–Kirchhoff stress tensor, S_{ij}^{PK2}, that can be expressed in vector form using Voigt notation as

$$\mathbf{S}_{\mathrm{PK2}} = [S_{11}^{\mathrm{PK2}}, S_{22}^{\mathrm{PK2}}, S_{33}^{\mathrm{PK2}}, S_{23}^{\mathrm{PK2}}, S_{13}^{\mathrm{PK2}}, S_{12}^{\mathrm{PK2}}]^{\mathrm{T}} \tag{10}$$

Copyright © 2006 John Wiley & Sons, Ltd.

DOI: 10.1002/nme

The Hu–Washizu functional in total Lagrangian formulation is [14]

$$\Pi_{\mathrm{HW}}(\mathbf{u}, \mathbf{S}_{\mathrm{PK2}}, \mathbf{E}_{\mathrm{G}}) = \int_{\Omega_0} \varphi(\mathbf{E}_{\mathrm{G}})\,\mathrm{d}\Omega_0 + \int_{\Omega_0} \mathbf{S}_{\mathrm{PK2}}^{\mathrm{T}}(\mathscr{H}\mathbf{u} - \mathbf{E}_{\mathrm{G}})\,\mathrm{d}\Omega_0 - \Pi_{\mathrm{ext}}(\mathbf{u}) \tag{11}$$

in which $\mathbf{u}$, $\mathbf{S}_{\mathrm{PK2}}$ and $\mathbf{E}_{\mathrm{G}}$ are the assumed displacement, stress and strain fields, respectively, $\varphi(\mathbf{E}_{\mathrm{G}})$ is the strain energy density and $\mathscr{H}$ is a differential matrix operator defined as

$$\mathscr{H} = \mathscr{H}_{\ell} + \tfrac{1}{2}\mathscr{H}_{n\ell} \tag{12}$$

$$\mathscr{H}_{\ell} = \begin{bmatrix} \dfrac{\partial}{\partial X_1} & 0 & 0 & 0 & \dfrac{\partial}{\partial X_3} & \dfrac{\partial}{\partial X_2} \\ 0 & \dfrac{\partial}{\partial X_2} & 0 & \dfrac{\partial}{\partial X_3} & 0 & \dfrac{\partial}{\partial X_1} \\ 0 & 0 & \dfrac{\partial}{\partial X_3} & \dfrac{\partial}{\partial X_2} & \dfrac{\partial}{\partial X_1} & 0 \end{bmatrix}^{\mathrm{T}} \tag{13}$$

$$\mathscr{H}_{n\ell} = \begin{bmatrix} \frac{\partial u_1}{\partial X_1}\frac{\partial}{\partial X_1} & \frac{\partial u_1}{\partial X_2}\frac{\partial}{\partial X_2} & \frac{\partial u_1}{\partial X_3}\frac{\partial}{\partial X_3} & \left(\frac{\partial u_1}{\partial X_2}\frac{\partial}{\partial X_3}+\frac{\partial u_1}{\partial X_3}\frac{\partial}{\partial X_2}\right) & \left(\frac{\partial u_1}{\partial X_1}\frac{\partial}{\partial X_3}+\frac{\partial u_1}{\partial X_3}\frac{\partial}{\partial X_1}\right) & \left(\frac{\partial u_1}{\partial X_1}\frac{\partial}{\partial X_2}+\frac{\partial u_1}{\partial X_2}\frac{\partial}{\partial X_1}\right) \\ \frac{\partial u_2}{\partial X_1}\frac{\partial}{\partial X_1} & \frac{\partial u_2}{\partial X_2}\frac{\partial}{\partial X_2} & \frac{\partial u_2}{\partial X_3}\frac{\partial}{\partial X_3} & \left(\frac{\partial u_2}{\partial X_2}\frac{\partial}{\partial X_3}+\frac{\partial u_2}{\partial X_3}\frac{\partial}{\partial X_2}\right) & \left(\frac{\partial u_2}{\partial X_1}\frac{\partial}{\partial X_3}+\frac{\partial u_2}{\partial X_3}\frac{\partial}{\partial X_1}\right) & \left(\frac{\partial u_2}{\partial X_1}\frac{\partial}{\partial X_2}+\frac{\partial u_2}{\partial X_2}\frac{\partial}{\partial X_1}\right) \\ \frac{\partial u_3}{\partial X_1}\frac{\partial}{\partial X_1} & \frac{\partial u_3}{\partial X_2}\frac{\partial}{\partial X_2} & \frac{\partial u_3}{\partial X_3}\frac{\partial}{\partial X_3} & \left(\frac{\partial u_3}{\partial X_2}\frac{\partial}{\partial X_3}+\frac{\partial u_3}{\partial X_3}\frac{\partial}{\partial X_2}\right) & \left(\frac{\partial u_3}{\partial X_1}\frac{\partial}{\partial X_3}+\frac{\partial u_3}{\partial X_3}\frac{\partial}{\partial X_1}\right) & \left(\frac{\partial u_3}{\partial X_1}\frac{\partial}{\partial X_2}+\frac{\partial u_3}{\partial X_2}\frac{\partial}{\partial X_1}\right) \end{bmatrix}^{\mathrm{T}} \tag{14}$$

where $\mathscr{H}_{\ell}$ and $\mathscr{H}_{n\ell}$ denote the linear and nonlinear parts, respectively, and the superposed T indicates the transpose operator. The term $\Pi_{\mathrm{ext}}(\mathbf{u})$ denotes the potential energy of the external forces and is defined as

$$\Pi_{\mathrm{ext}}(\mathbf{u}) = \int_{\Omega_0} \rho_0 \mathbf{b}^{\mathrm{T}}\mathbf{u}\,\mathrm{d}\Omega_0 + \int_{\partial\Omega_{0t}} \mathbf{t}_0^{\mathrm{T}}\mathbf{u}\,\mathrm{d}\Gamma_0 \tag{15}$$

where ρ denotes the mass density per unit volume, $\mathbf{b}$ are the body forces per unit mass, $\mathbf{t}$ are the surface tractions, $\partial\Omega_t$ denotes the part of the boundary $\partial\Omega$ of Ω where the surface tractions are prescribed, $\mathrm{d}\Omega$ and $\mathrm{d}\Gamma$ denote an infinitesimal volume and surface element, respectively, and the subscript '0' indicates that the quantities to which it is attached are computed in the reference configuration. For the sake of brevity, the term representing the kinetic energy is not included in the Hu–Washizu functional (Equation (11)). Notice that the kinetic energy term depends only on the displacement field and thus has the same form as in the case of the single-field (displacement-based) principle of virtual work [14].

Imposing the stationarity of the functional $\Pi_{\mathrm{HW}}(\mathbf{u}, \mathbf{S}_{\mathrm{PK2}}, \mathbf{E}_{\mathrm{G}})$ with respect to the three fields $\mathbf{u}$, $\mathbf{S}_{\mathrm{PK2}}$ and $\mathbf{E}_{\mathrm{G}}$ we obtain

$$\delta_{\mathbf{u}}\Pi_{\mathrm{HW}} = 0 \Rightarrow \int_{\Omega_0} (\mathscr{H}^{\mathrm{T}}\mathbf{S}_{\mathrm{PK2}} - \rho_0\mathbf{b})^{\mathrm{T}}\delta\mathbf{u}\,\mathrm{d}\Omega_0 - \int_{\partial\Omega_0 t} \mathbf{t}_0^{\mathrm{T}}\delta\mathbf{u}\,\mathrm{d}\Gamma_0 = 0 \tag{16}$$

Copyright © 2006 John Wiley & Sons, Ltd.

DOI: 10.1002/nme

$$\delta_{\mathbf{S}_{\mathrm{PK2}}}\Pi_{\mathrm{HW}}=0 \Rightarrow \int_{\Omega_0}(\mathscr{H}\mathbf{u}-\mathbf{E}_{\mathrm{G}})^{\mathrm{T}}\delta\mathbf{S}_{\mathrm{PK2}}\,\mathrm{d}\Omega_0=0 \tag{17}$$

$$\delta_{\mathbf{E}_{\mathrm{G}}}\Pi_{\mathrm{HW}}=0 \Rightarrow \int_{\Omega_0}\left(\frac{\partial\varphi(\mathbf{E}_{\mathrm{G}})}{\partial\mathbf{E}_{\mathrm{G}}}-\mathbf{S}_{\mathrm{PK2}}\right)^{\mathrm{T}}\delta\mathbf{E}_{\mathrm{G}}\,\mathrm{d}\Omega_0=0 \tag{18}$$

The classical Hu–Washizu formulation is limited to the case in which the strain energy density $\varphi(\mathbf{E}_{\mathrm{G}})$ is a potential, as for elastic materials. Equations (16)–(18) assume the meaning of weak forms of equilibrium, compatibility and constitutive law, respectively. In order to generalize the Hu–Washizu functional to the case of nonlinear inelastic materials, it is necessary to substitute the term $\partial\varphi(\mathbf{E}_{\mathrm{G}})/\partial\mathbf{E}_{\mathrm{G}}$ of the variation $\delta_{\mathbf{E}_{\mathrm{G}}}\Pi_{\mathrm{HW}}$ in Equation (18) with an expression for the second Piola–Kirchhoff stresses as a function of the Green–Lagrange strain history, i.e. $\hat{\mathbf{S}}_{\mathrm{PK2}}(\mathbf{E}_{\mathrm{G}})=\hat{\mathbf{S}}_{\mathrm{PK2}}(\mathbf{E}_{\mathrm{G}}(\tau),\,\tau\in[0,t])$ obtained through any material constitutive law. In the sequel, superposed hats, i.e. $\hat{\bullet}$, are placed on stress and stress-derived fields evaluated in terms of other independently interpolated variables (i.e. in terms of strains obtained from the assumed strain field) through the constitutive relations, while symbols without a superposed hat denote the assumed displacement, stress and strain fields. Thus, Equation (18) becomes

$$\delta_{\mathbf{E}_{\mathrm{G}}}\Pi_{\mathrm{HW}}=0 \Rightarrow \int_{\Omega_0}(\hat{\mathbf{S}}_{\mathrm{PK2}}(\mathbf{E}_{\mathrm{G}})-\mathbf{S}_{\mathrm{PK2}})^{\mathrm{T}}\delta\mathbf{E}_{\mathrm{G}}\,\mathrm{d}\Omega_0=0 \tag{19}$$

Introducing the finite element discretization and considering explicitly the dependencies on the sensitivity parameter θ, the mapping from the parent domain to the current configuration is given by

$$\mathbf{x}(\xi,\theta,t)=\mathbf{N}^e(\xi)\mathbf{x}_I^e(\theta,t) \tag{20}$$

and the mapping from the parent domain to the reference configuration is given by

$$\mathbf{X}(\xi,\theta)=\mathbf{N}^e(\xi)\mathbf{X}_I^e(\theta) \tag{21}$$

where $\mathbf{x}_I^e(\theta,t)$ and $\mathbf{X}_I^e(\theta)$ denote the coordinates of node I of element 'e' in the current configuration and reference configuration, respectively. In Equations (20) and (21), the parameter θ could represent a nodal coordinate in the reference configuration (shape parameter), for example. In the sequel, the dependency on time is not expressed explicitly in order to avoid a heavy notation and because it can be easily understood from the context. From the finite element discretization, the displacement, stress and strain fields are expressed as

$$\begin{aligned}\mathbf{u}^e(\xi,\theta) &= \mathbf{N}^e(\xi)\mathbf{q}^e(\theta)\\ \mathbf{S}_{\mathrm{PK2}}^e(\xi,\theta) &= \mathbf{S}^e(\xi)\mathbf{s}^e(\theta), \quad e=1,\ldots,N_{\mathrm{el}}\\ \mathbf{E}_{\mathrm{G}}^e(\xi,\theta) &= \mathbf{E}^e(\xi)\mathbf{e}^e(\theta)\end{aligned} \tag{22}$$

where $\mathbf{q}^e(\theta)$, $\mathbf{s}^e(\theta)$, and $\mathbf{e}^e(\theta)$ denote the nodal displacement, stress and strain parameters, respectively; $\mathbf{N}^e(\xi)$, $\mathbf{S}^e(\xi)$, and $\mathbf{E}^e(\xi)$ are the shape (interpolation) functions for the displacement, stress and strain fields, respectively, all quantities being referred to element 'e'; and N_{el} denotes the number of finite elements used discretizing the structure.

Copyright © 2006 John Wiley & Sons, Ltd.

DOI: 10.1002/nme

Substituting Equation (22) in Equations (16), (17) and (19), and recognizing that

$$\Omega_0 = \bigcup_{e=1}^{N_{\mathrm{el}}} \Omega_0^e \tag{23}$$

where $\bigcup$ denotes the union operator and Ω_0^e is the volume of the element 'e' in the reference configuration, we obtain the following weak forms of equilibrium, compatibility and constitutive law, respectively:

$$\sum_{e=1}^{N_{\mathrm{el}}} \left(\int_{\Omega_0^e} (\mathscr{H}^{\mathrm{T}} \mathbf{S}^e(\mathbf{X}) \mathbf{s}^e(\theta) - \rho_0(\mathbf{X}, \theta) \mathbf{b}(\mathbf{X}, \theta))^{\mathrm{T}} \cdot \mathbf{N}^e(\mathbf{X}) \, \mathrm{d}\Omega_0 \right.$$
$$\left. - \int_{\partial\Omega_{0t}^e} \mathbf{t}_0^{\mathrm{T}}(\mathbf{X}, \theta) \mathbf{N}^e(\mathbf{X}) \, \mathrm{d}\Gamma_0 \right) \delta \mathbf{q}^e = 0 \tag{24}$$

$$\sum_{e=1}^{N_{\mathrm{el}}} \left(\int_{\Omega_0^e} (\mathbf{E}^e(\mathbf{X}) \mathbf{e}^e(\theta) - \mathscr{H} \mathbf{N}^e(\mathbf{X}) \mathbf{q}^e(\theta))^{\mathrm{T}} \cdot \mathbf{S}^e(\mathbf{X}) \, \mathrm{d}\Omega_0 \right) \delta \mathbf{s}^e = 0 \tag{25}$$

$$\sum_{e=1}^{N_{\mathrm{el}}} \left(\int_{\Omega_0^e} (\mathbf{S}^e(\mathbf{X}) \mathbf{s}^e(\theta) - \hat{\mathbf{S}}_{\mathrm{PK2}}^e(\mathbf{E}^e(\mathbf{X}) \mathbf{e}^e(\theta), \theta))^{\mathrm{T}} \cdot \mathbf{E}^e(\mathbf{X}) \, \mathrm{d}\Omega_0 \right) \delta \mathbf{e}^e = 0 \tag{26}$$

Let us refer to a single element and drop the suffix 'e' in the sequel. Considering the arbitrary (virtual) nature of $\delta\mathbf{q}^e$, $\delta\mathbf{s}^e$, and $\delta\mathbf{e}^e$ in the above three equations, we obtain the following governing equations for each of the finite elements used in the discretization of the structural system:

$$\overline{\mathbf{B}}^{\mathrm{T}}(\theta) \mathbf{s}(\theta) - \mathbf{Q}(\theta) = \mathbf{0} \tag{27}$$

$$\overline{\mathbf{E}}(\theta) \mathbf{e}(\theta) - \overline{\mathbf{B}}(\theta) \mathbf{q}(\theta) = \mathbf{0} \tag{28}$$

$$\mathbf{a}(\mathbf{e}(\theta), \theta) - \overline{\mathbf{E}}^{\mathrm{T}}(\theta) \mathbf{s}(\theta) = \mathbf{0} \tag{29}$$

in which

$$\mathbf{Q}(\theta) = \int_{\Omega_0(\theta)} \rho_0(\mathbf{X}, \theta) \mathbf{b}^{\mathrm{T}}(\mathbf{X}, \theta) \mathbf{N}(\mathbf{X}) \, \mathrm{d}\Omega_0 + \int_{\partial\Omega_{0t}(\theta)} \mathbf{t}_0^{\mathrm{T}}(\mathbf{X}, \theta) \mathbf{N}(\mathbf{X}) \, \mathrm{d}\Gamma_0$$
$$= \int_{\square} \rho_0(\boldsymbol{\xi}, \theta) \mathbf{b}^{\mathrm{T}}(\boldsymbol{\xi}, \theta) \mathbf{N}(\boldsymbol{\xi}) J(\boldsymbol{\xi}, \theta) \, \mathrm{d}\square + \int_{\partial\square} \mathbf{t}_0^{\mathrm{T}}(\boldsymbol{\xi}, \theta) \mathbf{N}(\boldsymbol{\xi}) J(\boldsymbol{\xi}, \theta) \, \mathrm{d}(\partial\square) \tag{30}$$

$$\overline{\mathbf{B}}(\theta) = \int_{\Omega_0(\theta)} \mathbf{S}^{\mathrm{T}}(\mathbf{X}) \mathbf{B}(\mathbf{X}, \theta) \, \mathrm{d}\Omega_0 = \int_{\square} \mathbf{S}^{\mathrm{T}}(\boldsymbol{\xi}) \mathbf{B}(\boldsymbol{\xi}, \theta) J(\boldsymbol{\xi}, \theta) \, \mathrm{d}\square \tag{31}$$

$$\mathbf{B}(\boldsymbol{\xi}, \theta) = \mathscr{H}(\boldsymbol{\xi}, \theta) \mathbf{N}(\boldsymbol{\xi}) \tag{32}$$

Copyright © 2006 John Wiley & Sons, Ltd.

DOI: 10.1002/nme

$$\overline{\mathbf{E}}(\theta) = \int_{\Omega_0(\theta)} \mathbf{S}^{\mathrm{T}}(\mathbf{X})\mathbf{E}(\mathbf{X})\,\mathrm{d}\Omega_0 = \int_{\square} \mathbf{S}^{\mathrm{T}}(\boldsymbol{\xi})\mathbf{E}(\boldsymbol{\xi})\,J(\boldsymbol{\xi},\theta)\,\mathrm{d}\square \tag{33}$$

$$\begin{aligned}\mathbf{a}(\mathbf{e}(\theta),\theta) &= \int_{\Omega_0(\theta)} \mathbf{E}^{\mathrm{T}}(\mathbf{X})\hat{\mathbf{S}}_{\mathrm{PK2}}(\mathbf{E}(\mathbf{X})\mathbf{e}(\theta),\theta)\,\mathrm{d}\Omega_0 \\ &= \int_{\square} \mathbf{E}^{\mathrm{T}}(\boldsymbol{\xi})\hat{\mathbf{S}}_{\mathrm{PK2}}(\mathbf{E}(\boldsymbol{\xi})\mathbf{e}(\theta),\theta)\,J(\boldsymbol{\xi},\theta)\,\mathrm{d}\square\end{aligned} \tag{34}$$

where the symbol $\mathscr{H}(\boldsymbol{\xi},\theta)$ is used to highlight the dependency of the operator $\mathscr{H}$ on $\boldsymbol{\xi}$ and θ and $J(\boldsymbol{\xi},\theta)$ denotes the Jacobian of the transformation between the parent domain $\square$ and the reference domain Ω_0 such that $\mathrm{d}\Omega_0 = J(\boldsymbol{\xi},\theta)\cdot\mathrm{d}\square$, $\boldsymbol{\xi}\in\square$. Equations (27)–(29) constitute a system of $n_q+n_s+n_e$ coupled equations in $n_q+n_s+n_e$ unknowns, where n_q, n_s and n_e denotes the number of displacement, stress and strain parameters, respectively. Equation (29) is nonlinear if any of the used material models is nonlinear, Equations (27) and (28) are nonlinear since $\overline{\mathbf{B}}(\theta)$ depends on $\mathbf{q}(\theta)$ through the nonlinear part of the operator $\mathscr{H}(\boldsymbol{\xi},\theta)$ and $\mathbf{Q}(\theta)$ depends implicitly on $\mathbf{q}(\theta)$ when $\mathbf{t}_0$ is displacement-dependent. Notice that the surface tractions $\mathbf{t}_0$ at the element boundaries also contain the reactions of adjacent elements and thus are generally functions of the nodal displacements, i.e. $\mathbf{t}_0 = \mathbf{t}_0(\mathbf{q}(\theta),\theta)$. The nonlinear problem is solved using an incremental-iterative procedure, such as the Newton–Raphson method.

Differentiating Equation (28) exactly with respect to θ and performing some algebraic manipulations (see Appendix A), we obtain

$$\frac{\mathrm{d}\mathbf{e}(\theta)}{\mathrm{d}\theta} = \overline{\mathbf{D}}_t^{-1}(\theta)\overline{\mathbf{E}}^{\mathrm{T}}(\theta)\overline{\overline{\mathbf{D}}}_t^{-1}(\theta)\left(\overline{\mathbf{B}}(\theta)\frac{\mathrm{d}\mathbf{q}(\theta)}{\mathrm{d}\theta} + \frac{\mathrm{d}\overline{\mathbf{B}}(\theta)}{\mathrm{d}\theta}\mathbf{q}(\theta) - \frac{\mathrm{d}\overline{\mathbf{E}}(\theta)}{\mathrm{d}\theta}\mathbf{e}(\theta)\right) \tag{35}$$

in which the following matrices are introduced:

$$\overline{\mathbf{D}}_t(\theta) = \int_{\Omega_0(\theta)} \mathbf{E}^{\mathrm{T}}(\mathbf{X})\mathbf{k}_{\mathrm{IP}}(\mathbf{X})\mathbf{E}(\mathbf{X})\,\mathrm{d}\Omega_0 \tag{36}$$

$$\overline{\overline{\mathbf{D}}}_t(\theta) = \overline{\mathbf{E}}(\theta)\cdot\overline{\mathbf{D}}_t^{-1}(\theta)\cdot\overline{\mathbf{E}}^{\mathrm{T}}(\theta) \tag{37}$$

where $\mathbf{k}_{\mathrm{IP}}(\mathbf{X})$ denotes the material consistent (or algorithmic) tangent moduli at the integration point. Matrices $\overline{\mathbf{D}}_t(\theta)$ and $\overline{\overline{\mathbf{D}}}_t(\theta)$ are required in the element state determination for the response and in the response sensitivity computation. The reader is referred to Reference [16] for the conditions under which these two matrices are invertible assuming that $\mathbf{k}_{\mathrm{IP}}(\mathbf{X})$ is not singular.

Differentiating Equation $(22)_3$ and the material constitutive relation with respect to θ yields, respectively

$$\frac{\mathrm{d}\mathbf{E}_{\mathrm{G}}(\boldsymbol{\xi},\theta)}{\mathrm{d}\theta} = \mathbf{E}(\boldsymbol{\xi})\frac{\mathrm{d}\mathbf{e}(\theta)}{\mathrm{d}\theta} \tag{38}$$

Copyright © 2006 John Wiley & Sons, Ltd.

DOI: 10.1002/nme

$$\frac{\mathrm{d}\hat{\mathbf{S}}_{\mathrm{PK2}}(\xi,\theta)}{\mathrm{d}\theta} = \left.\frac{\partial\hat{\mathbf{S}}_{\mathrm{PK2}}(\xi,\theta)}{\partial\mathbf{E}_{\mathrm{G}}}\right|_{\theta}\frac{\mathrm{d}\mathbf{E}_{\mathrm{G}}(\xi,\theta)}{\mathrm{d}\theta} + \left.\frac{\partial\hat{\mathbf{S}}_{\mathrm{PK2}}(\xi,\theta)}{\partial\theta}\right|_{\mathbf{E}_{\mathrm{G}}}$$

$$= \mathbf{k}_{\mathrm{IP}}(\xi)\mathbf{E}(\xi)\frac{\mathrm{d}\mathbf{e}(\theta)}{\mathrm{d}\theta} + \left.\frac{\partial\hat{\mathbf{S}}_{\mathrm{PK2}}(\xi,\theta)}{\partial\theta}\right|_{\mathbf{e}} \tag{39}$$

Differentiating Equation (34) with respect to θ gives

$$\frac{\mathrm{d}\mathbf{a}(\mathbf{e}(\theta),\theta)}{\mathrm{d}\theta} = \int_{\square}\mathbf{E}^{\mathrm{T}}(\xi)\frac{\mathrm{d}\hat{\mathbf{S}}_{\mathrm{PK2}}(\xi,\theta)}{\mathrm{d}\theta}J(\xi,\theta)\,\mathrm{d}\square + \int_{\square}\mathbf{E}^{\mathrm{T}}(\xi)\hat{\mathbf{S}}_{\mathrm{PK2}}(\xi,\theta)\frac{\mathrm{d}J(\xi,\theta)}{\mathrm{d}\theta}\,\mathrm{d}\square \tag{40}$$

Equation (40) is obtained noting that, if $f(\mathbf{X},\theta)$ is a function defined in $\Omega_0(\theta)$ and $I(\theta)$ denotes the integral of this function over the reference domain, then

$$I(\theta) = \int_{\Omega_0(\theta)} f(\mathbf{X},\theta)\,\mathrm{d}\Omega_0 = \int_{\square} f(\xi,\theta)J(\xi,\theta)\,\mathrm{d}\square \tag{41}$$

from which

$$\frac{\mathrm{d}I(\theta)}{\mathrm{d}\theta} = \frac{\mathrm{d}}{\mathrm{d}\theta}\left(\int_{\square} f(\xi,\theta)J(\xi,\theta)\,\mathrm{d}\square\right) = \int_{\square}\frac{\mathrm{d}}{\mathrm{d}\theta}[f(\xi,\theta)J(\xi,\theta)]\,\mathrm{d}\square$$

$$= \int_{\square}\frac{\mathrm{d}f(\xi,\theta)}{\mathrm{d}\theta}J(\xi,\theta)\,\mathrm{d}\square + \int_{\square} f(\xi,\theta)\frac{\mathrm{d}J(\xi,\theta)}{\mathrm{d}\theta}\,\mathrm{d}\square \tag{42}$$

Finally, by differentiating Equations (29) and (27) with respect to θ and performing some algebraic manipulations (see Appendix A), we obtain, respectively,

$$\frac{\mathrm{d}\mathbf{s}(\mathbf{e}(\theta),\theta)}{\mathrm{d}\theta} = \overline{\overline{\mathbf{D}}}_t^{-1}(\theta)\overline{\mathbf{E}}(\theta)\overline{\mathbf{D}}_t^{-1}(\theta)\left(\frac{\mathrm{d}\mathbf{a}(\mathbf{e}(\theta),\theta)}{\mathrm{d}\theta} - \frac{\mathrm{d}(\overline{\mathbf{E}}^{\mathrm{T}}(\theta))}{\mathrm{d}\theta}\mathbf{s}(\mathbf{e}(\theta),\theta)\right) \tag{43}$$

$$\frac{\mathrm{d}\mathbf{Q}(\mathbf{e}(\theta),\theta)}{\mathrm{d}\theta} = \overline{\mathbf{B}}^{\mathrm{T}}(\theta)\frac{\mathrm{d}\mathbf{s}(\mathbf{e}(\theta),\theta)}{\mathrm{d}\theta} + \frac{\mathrm{d}(\overline{\mathbf{B}}^{\mathrm{T}}(\theta))}{\mathrm{d}\theta}\mathbf{s}(\mathbf{e}(\theta),\theta) \tag{44}$$

In order to compute the conditional response sensitivities (for $\mathbf{q}$ fixed, thus with $\partial\mathbf{q}(\theta)/\partial\theta|_{\mathbf{q}} = \mathbf{0}$), Equations (35), (38)–(40), (43) and (44) are modified as

$$\left.\frac{\partial\mathbf{e}(\theta)}{\partial\theta}\right|_{\mathbf{q}} = \overline{\mathbf{D}}_t^{-1}(\theta)\overline{\mathbf{E}}^{\mathrm{T}}(\theta)\overline{\overline{\mathbf{D}}}_t^{-1}(\theta)\left(\left.\frac{\partial\overline{\mathbf{B}}(\theta)}{\partial\theta}\right|_{\mathbf{q}}\mathbf{q}(\theta) - \frac{\mathrm{d}\overline{\mathbf{E}}(\theta)}{\mathrm{d}\theta}\mathbf{e}(\theta)\right) \tag{45}$$

$$\left.\frac{\partial\mathbf{E}_{\mathrm{G}}(\xi,\theta)}{\partial\theta}\right|_{\mathbf{q}} = \mathbf{E}(\xi)\left.\frac{\partial\mathbf{e}(\theta)}{\partial\theta}\right|_{\mathbf{q}} \tag{46}$$

$$\left.\frac{\partial\hat{\mathbf{S}}_{\mathrm{PK2}}(\xi,\theta)}{\partial\theta}\right|_{\mathbf{q}} = \mathbf{k}_{\mathrm{IP}}(\xi)\mathbf{E}(\xi)\left.\frac{\partial\mathbf{e}(\theta)}{\partial\theta}\right|_{\mathbf{q}} + \left.\frac{\partial\hat{\mathbf{S}}_{\mathrm{PK2}}(\xi,\theta)}{\partial\theta}\right|_{\mathbf{e},\mathbf{q}} \tag{47}$$

Copyright © 2006 John Wiley & Sons, Ltd.

DOI: 10.1002/nme

$$\left.\frac{\partial \mathbf{a}(\mathbf{e}(\theta),\theta)}{\partial\theta}\right|_{\mathbf{q}} = \int_{\square} \mathbf{E}^{\mathrm{T}}(\xi)\left.\frac{\partial \hat{\mathbf{S}}_{\mathrm{PK2}}(\xi,\theta)}{\partial\theta}\right|_{\mathbf{q}} J(\xi,\theta)\,\mathrm{d}\square + \int_{\square} \mathbf{E}^{\mathrm{T}}(\xi)\hat{\mathbf{S}}_{\mathrm{PK2}}(\xi,\theta)\frac{\mathrm{d}J(\xi,\theta)}{\mathrm{d}\theta}\,\mathrm{d}\square \tag{48}$$

$$\left.\frac{\partial \mathbf{s}(\mathbf{e}(\theta),\theta)}{\partial\theta}\right|_{\mathbf{q}} = \overline{\overline{\mathbf{D}}}_t^{-1}(\theta)\overline{\mathbf{E}}(\theta)\overline{\mathbf{D}}_t^{-1}(\theta)\left(\left.\frac{\partial \mathbf{a}(\mathbf{e}(\theta),\theta)}{\partial\theta}\right|_{\mathbf{q}} - \frac{\mathrm{d}(\overline{\mathbf{E}}^{\mathrm{T}}(\theta))}{\mathrm{d}\theta}\mathbf{s}(\mathbf{e}(\theta),\theta)\right) \tag{49}$$

$$\left.\frac{\partial \mathbf{Q}(\mathbf{e}(\theta),\theta)}{\partial\theta}\right|_{\mathbf{q}} = \overline{\mathbf{B}}^{\mathrm{T}}(\theta)\left.\frac{\partial \mathbf{s}(\mathbf{e}(\theta),\theta)}{\partial\theta}\right|_{\mathbf{q}} + \left.\frac{\partial(\overline{\mathbf{B}}^{\mathrm{T}}(\theta))}{\partial\theta}\right|_{\mathbf{q}} \mathbf{s}(\mathbf{e}(\theta),\theta) \tag{50}$$

where the quantity $\partial\hat{\mathbf{S}}_{\mathrm{PK2}}(\xi,\theta)/\partial\theta|_{\mathbf{e},\mathbf{q}}$ in Equation (47) is computed through conditional differentiation (at the material level) of the material constitutive law. Note that $\overline{\mathbf{E}}(\theta)$ depends on θ only through $\Omega_0(\theta)$, and thus $\mathrm{d}\overline{\mathbf{E}}(\theta)/\mathrm{d}\theta = \partial\overline{\mathbf{E}}(\theta)/\partial\theta|_{\mathbf{q}}$. Furthermore, $\mathbf{e}(\theta)$ depends on θ both explicitly and implicitly through $\mathbf{q}(\theta)$, i.e. $\mathbf{e}(\theta) = \mathbf{e}(\mathbf{q}(\theta),\theta)$, as shown in Equation (35). The quantities $\mathbf{s}(\theta)$ and $\mathbf{Q}(\theta)$ also depend on θ both explicitly and implicitly through $\mathbf{e}(\theta)$, since they are functions of $\mathbf{a}(\mathbf{e}(\theta),\theta)$ as shown in Equations (43) and (44).

3.2. Specialization to geometric linear formulation

If linear geometry (i.e. small displacements and small strains) is assumed, the three-field mixed finite element formulation can be obtained from the stationarity conditions of the Hu–Washizu functional, that can be written as [11]

$$\Pi_{\mathrm{HW}}(\mathbf{u},\boldsymbol{\sigma},\boldsymbol{\varepsilon}) = \int_{\Omega}\varphi(\boldsymbol{\varepsilon})\,\mathrm{d}\Omega + \int_{\Omega}\boldsymbol{\sigma}^{\mathrm{T}}(\mathscr{D}\mathbf{u}-\boldsymbol{\varepsilon})\,\mathrm{d}\Omega - \Pi_{\mathrm{ext}}(\mathbf{u}) \tag{51}$$

where $\mathbf{u}$, $\boldsymbol{\sigma}$ and $\boldsymbol{\varepsilon}$ are the assumed displacement, stress and (small) strain fields, respectively, $\varphi(\boldsymbol{\varepsilon})$ is the strain energy density, $\mathscr{D}$ is a linear differential operator matrix defined as

$$\mathscr{D} = \begin{bmatrix} \frac{\partial}{\partial X_1} & 0 & 0 & 0 & \frac{\partial}{\partial X_3} & \frac{\partial}{\partial X_2} \\ 0 & \frac{\partial}{\partial X_2} & 0 & \frac{\partial}{\partial X_3} & 0 & \frac{\partial}{\partial X_1} \\ 0 & 0 & \frac{\partial}{\partial X_3} & \frac{\partial}{\partial X_2} & \frac{\partial}{\partial X_1} & 0 \end{bmatrix}^{\mathrm{T}} \tag{52}$$

As in the previous section, matrix notation and Voigt notation are used [14] here. The term $\Pi_{\mathrm{ext}}(\mathbf{u})$ denotes the potential energy of the external forces and is defined as

$$\Pi_{\mathrm{ext}}(\mathbf{u}) = \int_{\Omega}\mathbf{b}^{\mathrm{T}}\mathbf{u}\,\mathrm{d}\Omega + \int_{\partial\Omega_t}\mathbf{t}^{\mathrm{T}}\mathbf{u}\,\mathrm{d}\Gamma \tag{53}$$

As in the general formulation presented in previous section, the term representing the kinetic energy is not included in the Hu–Washizu functional in Equation (51).

Copyright © 2006 John Wiley & Sons, Ltd.

DOI: 10.1002/nme

Imposing stationarity of the Hu–Washizu functional in Equation (51) with respect to the three fields $\mathbf{u}$, $\boldsymbol{\sigma}$ and $\boldsymbol{\varepsilon}$, yields

$$\delta_{\mathbf{u}}\Pi_{\mathrm{HW}} = 0 \;\Rightarrow\; \int_{\Omega} (\mathscr{D}^{\mathrm{T}}\boldsymbol{\sigma} - \mathbf{b})^{\mathrm{T}}\delta\mathbf{u}\,\mathrm{d}\Omega - \int_{\partial\Omega_t} \mathbf{t}^{\mathrm{T}}\delta\mathbf{u}\,\mathrm{d}\Gamma = 0 \tag{54}$$

$$\delta_{\boldsymbol{\sigma}}\Pi_{\mathrm{HW}} = 0 \;\Rightarrow\; \int_{\Omega} (\mathscr{D}\mathbf{u} - \boldsymbol{\varepsilon})^{\mathrm{T}}\delta\boldsymbol{\sigma}\,\mathrm{d}\Omega = 0 \tag{55}$$

$$\delta_{\boldsymbol{\varepsilon}}\Pi_{\mathrm{HW}} = 0 \;\Rightarrow\; \int_{\Omega} \left(\frac{\partial\varphi(\boldsymbol{\varepsilon})}{\partial\boldsymbol{\varepsilon}} - \boldsymbol{\sigma}\right)^{\mathrm{T}} \delta\boldsymbol{\varepsilon}\,\mathrm{d}\Omega = 0 \tag{56}$$

The classical Hu–Washizu formulation is limited to the case in which the strain energy density $\varphi(\boldsymbol{\varepsilon})$ is a potential, as for elastic materials. Equations (54)–(56) assume the meaning of weak forms of equilibrium, compatibility and constitutive law, respectively. In order to generalize the Hu–Washizu functional to the case of nonlinear inelastic materials, it is necessary to substitute the term $\partial\varphi(\boldsymbol{\varepsilon})/\partial\boldsymbol{\varepsilon}$ of the variation $\delta_{\boldsymbol{\varepsilon}}\Pi_{\mathrm{HW}}$ in Equation (56) with an expression for the stresses as a function of the strain history, i.e. $\hat{\boldsymbol{\sigma}}(\boldsymbol{\varepsilon}) = \hat{\boldsymbol{\sigma}}(\boldsymbol{\varepsilon}(\tau), \tau \in [0, t])$, obtained through any material constitutive law (see Section 3.1).

The finite element approximations of the three independently interpolated fields $\mathbf{u}$, $\boldsymbol{\sigma}$ and $\boldsymbol{\varepsilon}$ take the form, respectively,

$$\begin{aligned} \mathbf{u}^e(\mathbf{X}, \theta) &= \mathbf{N}^e(\mathbf{X})\mathbf{q}^e(\theta) \\ \boldsymbol{\sigma}^e(\mathbf{X}, \theta) &= \mathbf{S}^e(\mathbf{X})\mathbf{s}^e(\theta), \quad e = 1, \ldots, N_{\mathrm{el}} \\ \boldsymbol{\varepsilon}^e(\mathbf{X}, \theta) &= \mathbf{E}^e(\mathbf{X})\mathbf{e}^e(\theta) \end{aligned} \tag{57}$$

Henceforth, the dependencies of the different quantities on the sensitivity parameter θ and on the position vector $\mathbf{X} = [X_1, X_2, X_3]^{\mathrm{T}}$ are shown explicitly because of their important role in the derivation of the response sensitivity equations. Unlike in Section 3.1, relations for shape sensitivity computations are not derived; they would require considering the dependencies of shape functions and integration domains on the sensitivity parameter θ.

Substituting Equation (57) in Equations (54)–(56), we obtain the following weak forms of equilibrium, compatibility and constitutive law, respectively:

$$\sum_{e=1}^{N_{el}} \left(\int_{\Omega^e} (\mathscr{D}^{\mathrm{T}}\mathbf{S}^e(\mathbf{X})\mathbf{s}^e(\theta) - \mathbf{b}^e(\mathbf{X}))^{\mathrm{T}} \cdot \mathbf{N}^e(\mathbf{X})\,\mathrm{d}\Omega - \int_{\partial\Omega_t^e} \mathbf{t}^{\mathrm{T}}(\mathbf{X})\mathbf{N}^e(\mathbf{X})\,\mathrm{d}\Gamma \right) \delta\mathbf{q}^e = 0 \tag{58}$$

$$\sum_{e=1}^{N_{el}} \left(\int_{\Omega^e} (\mathbf{E}^e(\mathbf{X})\mathbf{e}^e(\theta) - \mathscr{D}\mathbf{N}^e(\mathbf{X})\mathbf{q}^e(\theta))^{\mathrm{T}} \cdot \mathbf{S}^e(\mathbf{X})\,\mathrm{d}\Omega \right) \delta\mathbf{s}^e = 0 \tag{59}$$

$$\sum_{e=1}^{N_{el}} \left(\int_{\Omega^e} (\mathbf{S}^e(\mathbf{X})\mathbf{s}^e(\theta) - \hat{\boldsymbol{\sigma}}^e(\mathbf{E}^e(\mathbf{X})\mathbf{e}^e(\theta), \theta))^{\mathrm{T}} \cdot \mathbf{E}^e(\mathbf{X})\,\mathrm{d}\Omega \right) \delta\mathbf{e}^e = 0 \tag{60}$$

Let us define $\mathbf{B}^e(\mathbf{X}) = \mathscr{D}\mathbf{N}^e(\mathbf{X})$ and drop the suffix 'e' in the sequel. Considering the arbitrary (virtual) nature of $\delta\mathbf{q}^e$, $\delta\mathbf{s}^e$, and $\delta\mathbf{e}^e$ in Equations (58)–(60), we obtain the following governing

Copyright © 2006 John Wiley & Sons, Ltd.

DOI: 10.1002/nme

equations for each of the finite elements used in the discretization of the structural system:

$$\overline{\mathbf{B}}^{\mathrm{T}}\mathbf{s}(\theta) - \mathbf{Q}(\theta) = \mathbf{0} \tag{61}$$

$$\overline{\mathbf{E}}\mathbf{e}(\theta) - \overline{\mathbf{B}}\mathbf{q}(\theta) = \mathbf{0} \tag{62}$$

$$\mathbf{a}(\mathbf{e}(\theta), \theta) - \overline{\mathbf{E}}^{\mathrm{T}}\mathbf{s}(\theta) = \mathbf{0} \tag{63}$$

where

$$\mathbf{Q}(\theta) = \int_{\Omega} \mathbf{b}^{\mathrm{T}}(\mathbf{X}, \theta)\mathbf{N}(\mathbf{X})\,\mathrm{d}\Omega + \int_{\partial\Omega_t} \mathbf{t}^{\mathrm{T}}(\mathbf{X}, \theta)\mathbf{N}(\mathbf{X})\,\mathrm{d}\Gamma \tag{64}$$

$$\overline{\mathbf{B}} = \int_{\Omega} \mathbf{S}^{\mathrm{T}}(\mathbf{X})\mathbf{B}(\mathbf{X})\,\mathrm{d}\Omega \tag{65}$$

$$\overline{\mathbf{E}} = \int_{\Omega} \mathbf{S}^{\mathrm{T}}(\mathbf{X})\mathbf{E}(\mathbf{X})\,\mathrm{d}\Omega \tag{66}$$

$$\mathbf{a}(\mathbf{e}(\theta), \theta) = \int_{\Omega} \mathbf{E}^{\mathrm{T}}(\mathbf{X})\hat{\boldsymbol{\sigma}}(\mathbf{E}(\mathbf{X})\mathbf{e}(\theta), \theta)\,\mathrm{d}\Omega \tag{67}$$

Equations (61)–(63) represent a system of $n_q + n_s + n_e$ (generally) coupled equations in $n_q + n_s + n_e$ unknowns, where n_q, n_s and n_e denote the number of displacement, stress and strain parameters, respectively. Equations (61) and (62) are linear, while Equation (63) is nonlinear if any of the used material models is nonlinear. The nonlinear problem is solved using an incremental-iterative scheme, such as the Newton–Raphson method. In some special cases the matrix $\overline{\mathbf{E}}$ is invertible (e.g. when the stress shape functions $\mathbf{S}(\mathbf{X})$ and strain shape functions $\mathbf{E}(\mathbf{X})$ are identical) [16] and Equations (61)–(63) can be uncoupled and solved sequentially. However, the general case is considered hereunder, while a special case for which the matrix $\overline{\mathbf{E}}$ is invertible will be presented later for a specific finite element implementation (Section 4.1).

Differentiating Equation (62) with respect to θ and premultiplying by $\overline{\mathbf{D}}_t^{-1}\overline{\mathbf{E}}^{\mathrm{T}}\overline{\overline{\mathbf{D}}}_t^{-1}$ yields the following relation, after some algebraic manipulations (see Appendix A):

$$\frac{\mathrm{d}\mathbf{e}(\theta)}{\mathrm{d}\theta} = \overline{\mathbf{D}}_t^{-1}\overline{\mathbf{E}}^{\mathrm{T}}\overline{\overline{\mathbf{D}}}_t^{-1}\overline{\mathbf{B}}\frac{\mathrm{d}\mathbf{q}(\theta)}{\mathrm{d}\theta} \tag{68}$$

where, similarly as in the previous section, matrices $\overline{\mathbf{D}}_t$ and $\overline{\overline{\mathbf{D}}}_t$ are defined as

$$\overline{\mathbf{D}}_t = \int_{\Omega} \mathbf{E}^{\mathrm{T}}(\mathbf{X})\mathbf{k}_{\mathrm{IP}}(\mathbf{X})\mathbf{E}(\mathbf{X})\,\mathrm{d}\Omega \tag{69}$$

$$\overline{\overline{\mathbf{D}}}_t = \overline{\mathbf{E}}\overline{\mathbf{D}}_t^{-1}\overline{\mathbf{E}}^{\mathrm{T}} \tag{70}$$

These matrices are required in the element state determination for the response and in the response sensitivity computation. The reader is referred to Reference [16] for the conditions under which these two matrices are invertible assuming that $\mathbf{k}_{\mathrm{IP}}(\mathbf{X})$ is not singular.

Copyright © 2006 John Wiley & Sons, Ltd.

DOI: 10.1002/nme

Differentiating Equation $(57)_3$ and the material constitutive relation with respect to θ yields, respectively,

$$\frac{\mathrm{d}\boldsymbol{\varepsilon}(\mathbf{X},\theta)}{\mathrm{d}\theta}=\mathbf{E}(\mathbf{X})\frac{\mathrm{d}\mathbf{e}(\theta)}{\mathrm{d}\theta} \tag{71}$$

$$\frac{\mathrm{d}\hat{\boldsymbol{\sigma}}(\mathbf{X},\theta)}{\mathrm{d}\theta}=\left.\frac{\partial\hat{\boldsymbol{\sigma}}(\mathbf{X},\theta)}{\partial\boldsymbol{\varepsilon}}\right|_{\theta}\frac{\mathrm{d}\boldsymbol{\varepsilon}(\mathbf{X},\theta)}{\mathrm{d}\theta}+\left.\frac{\partial\hat{\boldsymbol{\sigma}}(\mathbf{X},\theta)}{\partial\theta}\right|_{\boldsymbol{\varepsilon}}=\mathbf{k}_{\mathrm{IP}}(\mathbf{X})\mathbf{E}(\mathbf{X})\frac{\mathrm{d}\mathbf{e}(\theta)}{\mathrm{d}\theta}+\left.\frac{\partial\hat{\boldsymbol{\sigma}}(\mathbf{X},\theta)}{\partial\theta}\right|_{\mathbf{e}} \tag{72}$$

Differentiating Equation (67) with respect to θ and substituting Equations (72) and (69) in the resulting equation gives

$$\frac{\mathrm{d}\mathbf{a}(\mathbf{e}(\theta),\theta)}{\mathrm{d}\theta}=\int_{\Omega}\mathbf{E}^{\mathrm{T}}(\mathbf{X})\frac{\mathrm{d}\hat{\boldsymbol{\sigma}}(\mathbf{X},\theta)}{\mathrm{d}\theta}\,\mathrm{d}\Omega=\overline{\mathbf{D}}_t\frac{\mathrm{d}\mathbf{e}(\theta)}{\mathrm{d}\theta}+\int_{\Omega}\mathbf{E}^{\mathrm{T}}(\mathbf{X})\left.\frac{\partial\hat{\boldsymbol{\sigma}}(\mathbf{X},\theta)}{\partial\theta}\right|_{\mathbf{e}}\mathrm{d}\Omega \tag{73}$$

Finally, by differentiating Equations (63) and (61) with respect to θ and performing some algebraic manipulations (see Appendix A), we obtain, respectively,

$$\frac{\mathrm{d}\mathbf{s}(\mathbf{e}(\theta),\theta)}{\mathrm{d}\theta}=\overline{\overline{\mathbf{D}}}_t^{-1}\overline{\mathbf{E}}\overline{\mathbf{D}}_t^{-1}\frac{\mathrm{d}\mathbf{a}(\mathbf{e}(\theta),\theta)}{\mathrm{d}\theta} \tag{74}$$

$$\frac{\mathrm{d}\mathbf{Q}(\mathbf{e}(\theta),\theta)}{\mathrm{d}\theta}=\overline{\mathbf{B}}^{\mathrm{T}}\frac{\mathrm{d}\mathbf{s}(\mathbf{e}(\theta),\theta)}{\mathrm{d}\theta} \tag{75}$$

In order to compute the conditional response sensitivities (for $\mathbf{q}$ fixed, thus with $\partial\mathbf{q}(\theta)/\partial\theta|_{\mathbf{q}}=\mathbf{0}$), Equations (68) and (71)–(75) are modified as

$$\left.\frac{\partial\mathbf{e}(\theta)}{\partial\theta}\right|_{\mathbf{q}}=\mathbf{0} \tag{76}$$

$$\left.\frac{\partial\boldsymbol{\varepsilon}(\mathbf{X},\theta)}{\partial\theta}\right|_{\mathbf{q}}=\mathbf{0} \tag{77}$$

$$\left.\frac{\partial\hat{\boldsymbol{\sigma}}(\mathbf{X},\theta)}{\partial\theta}\right|_{\mathbf{q}}=\left.\frac{\partial\hat{\boldsymbol{\sigma}}(\mathbf{X},\theta)}{\partial\theta}\right|_{\mathbf{e}} \tag{78}$$

$$\left.\frac{\partial\mathbf{a}(\mathbf{e}(\theta),\theta)}{\partial\theta}\right|_{\mathbf{q}}=\int_{\Omega}\mathbf{E}^{\mathrm{T}}(\mathbf{X})\left.\frac{\partial\hat{\boldsymbol{\sigma}}(\mathbf{X},\theta)}{\partial\theta}\right|_{\mathbf{q}}\mathrm{d}\Omega \tag{79}$$

$$\left.\frac{\partial\mathbf{s}(\mathbf{e}(\theta),\theta)}{\partial\theta}\right|_{\mathbf{q}}=\overline{\overline{\mathbf{D}}}_t^{-1}\overline{\mathbf{E}}\overline{\mathbf{D}}_t^{-1}\left.\frac{\partial\mathbf{a}(\mathbf{e}(\theta),\theta)}{\partial\theta}\right|_{\mathbf{q}} \tag{80}$$

$$\left.\frac{\partial\mathbf{Q}(\mathbf{e}(\theta),\theta)}{\partial\theta}\right|_{\mathbf{q}}=\overline{\mathbf{B}}^{\mathrm{T}}\left.\frac{\partial\mathbf{s}(\mathbf{e}(\theta),\theta)}{\partial\theta}\right|_{\mathbf{q}} \tag{81}$$

Copyright © 2006 John Wiley & Sons, Ltd.

DOI: 10.1002/nme

where the quantity $\partial\hat{\boldsymbol{\sigma}}(\mathbf{X}, \theta)/\partial\theta|_{\mathbf{e}}$ in Equation (78) is computed by conditional differentiation (at the material level) of the material constitutive law. It is noteworthy that, in the case of linear geometry, assuming $\mathbf{q}$ fixed is equivalent to assuming $\mathbf{e}$ fixed ($\mathbf{e}$ and $\mathbf{q}$ are linearly related as shown by Equations (62) and (68)), while this equivalence does not apply in the case of nonlinear geometry (see Equations (28) and (35)).

3.3. Specialization to 2-D frame structures

As already discussed in Section 1, the frame element is an important class of finite elements for which the beneficial effects of a multi-field mixed formulation have been studied, proved and employed. The specialization of the above three-field mixed formulation to 2-D frame elements requires the definition of the section deformation vector, $\mathbf{d}$, and section stress resultant vector, $\mathbf{D}$. The explicit definition of the above vectors depends on the specific frame element considered. In general, a matrix $\mathbf{A}_s(\mathbf{X})$ can be defined such that

$$\boldsymbol{\varepsilon}(\mathbf{X}, \theta) = \mathbf{A}_s(\mathbf{X})\mathbf{d}(x, \theta) \tag{82}$$

$$\mathbf{D}(x, \theta) = \int_{A(x)} \mathbf{A}_s(\mathbf{X})^{\mathrm{T}}\boldsymbol{\sigma}(\mathbf{X}, \theta)\,\mathrm{d}A \tag{83}$$

where x denotes the abscissa along the frame axis ($x \in [0, L]$, L the length of the frame element) and $A(x)$ denotes the cross-section at abscissa x. Explicit expressions for $\mathbf{d}$, $\mathbf{D}$, and $\mathbf{A}_s(\mathbf{X})$ corresponding to common frame models presented in the literature are given in Appendix B. In this section and in Appendix B, the notation $\mathbf{X} = [X_1, X_2, X_3]^{\mathrm{T}} = [x, y, z]^{\mathrm{T}}$ is employed for consistency with the majority of the literature on frame elements.

For frame finite elements, it is common to use shape functions directly for the previously defined quantities $\mathbf{d}$ and $\mathbf{D}$ and to obtain the complete displacement fields from the displacements $\mathbf{u}(x, \theta)$ of the reference axis of the frame. Thus, Equation (57) can be rewritten as

$$\begin{aligned} \mathbf{u}(x, \theta) &= \mathbf{N}(x)\mathbf{q}(\theta) \\ \mathbf{D}(x, \theta) &= \mathbf{S}(x)\mathbf{s}(\theta) \\ \mathbf{d}(x, \theta) &= \mathbf{E}(x)\mathbf{e}(\theta) \end{aligned} \tag{84}$$

Accounting for Equations (82)–(84), all the theoretical developments presented in the previous sections for both response and response sensitivity analysis can be directly applied to any frame element treated in the context of a three-field mixed formulation. In particular, the governing equations for a frame element are formally identical to Equations (61)–(63), when the following specialized definitions are used:

$$\mathbf{Q}(\theta) = \int_0^L \mathbf{b}^{\mathrm{T}}(x)\mathbf{N}(x)\,\mathrm{d}x + [\mathbf{t}^{\mathrm{T}}(x)\mathbf{N}(x)]|_{x=0}^{x=L} \tag{85}$$

$$\overline{\mathbf{B}} = \int_0^L \mathbf{S}^{\mathrm{T}}(x)\mathbf{B}(x)\,\mathrm{d}x \tag{86}$$

Copyright © 2006 John Wiley & Sons, Ltd.

DOI: 10.1002/nme

$$\overline{\mathbf{E}} = \int_0^L \mathbf{S}^{\mathrm{T}}(x)\mathbf{E}(x)\,\mathrm{d}x \tag{87}$$

$$\mathbf{a}(\mathbf{e}(\theta), \theta) = \int_0^L \mathbf{E}^{\mathrm{T}}(x)\hat{\mathbf{D}}(\mathbf{E}(x)\mathbf{e}(\theta), \theta)\,\mathrm{d}x \tag{88}$$

$$\overline{\mathbf{D}}_t = \int_0^L \mathbf{E}^{\mathrm{T}}(x)\mathbf{k}_s(x)\mathbf{E}(x)\,\mathrm{d}x \tag{89}$$

where $\mathbf{k}_s(x)$ denotes the consistent tangent stiffness matrix of the section at the abscissa x.

The sensitivity Equations (68) and (71)–(75) specialize to

$$\frac{\mathrm{d}\mathbf{e}(\theta)}{\mathrm{d}\theta} = \overline{\mathbf{D}}_t^{-1}\overline{\mathbf{E}}^{\mathrm{T}}\overline{\overline{\mathbf{D}}}_t^{-1}\overline{\mathbf{B}}\frac{\mathrm{d}\mathbf{q}(\theta)}{\mathrm{d}\theta} \tag{90}$$

$$\frac{\mathrm{d}\mathbf{d}(x, \theta)}{\mathrm{d}\theta} = \mathbf{E}(x)\frac{\mathrm{d}\mathbf{e}(\theta)}{\mathrm{d}\theta} \tag{91}$$

$$\frac{\mathrm{d}\hat{\mathbf{D}}(x, \theta)}{\mathrm{d}\theta} = \mathbf{k}_s(x)\mathbf{E}(x)\frac{\mathrm{d}\mathbf{e}(\theta)}{\mathrm{d}\theta} + \left.\frac{\partial\hat{\mathbf{D}}(x, \theta)}{\partial\theta}\right|_{\mathbf{e}} \tag{92}$$

$$\frac{\mathrm{d}\mathbf{a}(\mathbf{e}(\theta), \theta)}{\mathrm{d}\theta} = \overline{\mathbf{D}}_t\frac{\mathrm{d}\mathbf{e}(\theta)}{\mathrm{d}\theta} + \int_0^L \mathbf{E}^{\mathrm{T}}(x)\left.\frac{\partial\hat{\mathbf{D}}(x, \theta)}{\partial\theta}\right|_{\mathbf{e}}\mathrm{d}x \tag{93}$$

$$\frac{\mathrm{d}\mathbf{s}(\mathbf{e}(\theta), \theta)}{\mathrm{d}\theta} = \overline{\overline{\mathbf{D}}}_t^{-1}\overline{\mathbf{E}}\overline{\mathbf{D}}_t^{-1}\frac{\mathrm{d}\mathbf{a}(\mathbf{e}(\theta), \theta)}{\mathrm{d}\theta} \tag{94}$$

$$\frac{\mathrm{d}\mathbf{Q}(\mathbf{e}(\theta), \theta)}{\mathrm{d}\theta} = \overline{\mathbf{B}}^{\mathrm{T}}\frac{\mathrm{d}\mathbf{s}(\mathbf{e}(\theta), \theta)}{\mathrm{d}\theta} \tag{95}$$

The equations for conditional response sensitivity computation are readily obtained from Equations (90)–(95) imposing $\partial\mathbf{q}(\theta)/\partial\theta|_{\mathbf{q}} = \mathbf{0}$ and computing all the derivatives for $\mathbf{q}$ fixed, as seen in Section 3.2 (Equations (76)–(81)).

4. VALIDATION EXAMPLES

4.1. Finite element modelling of steel–concrete composite frame structures

Composite frames made of steel–concrete beams and steel columns are nowadays common solutions in the design of seismic resistant frames. As a consequence, in the last 10 years, a growing attention has been given to finite element modelling and analysis of steel–concrete composite structures [25]. The behaviour of composite beams, consisting of two components connected through shear connectors to form an interacting unit, is significantly influenced by

Copyright © 2006 John Wiley & Sons, Ltd.

DOI: 10.1002/nme

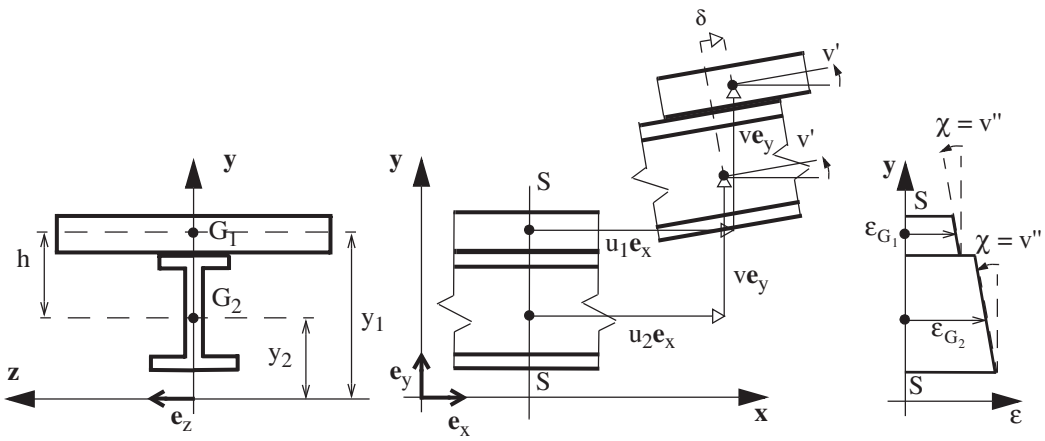

Figure 1. Kinematics of 2-D composite beam model (Newmark's model).

the type of connection between the steel beam and the concrete slab. Partial composite action develops when using flexible shear connectors [26]. Thus, for accurate analytical predictions, structural models of composite structures must account for the interlayer slip between the steel and concrete components. For this reason, a composite beam finite element able to model the effects of the interface slip is required. The three-dimensional model for composite beams with deformable shear connection under general state of stress [27] simplifies to the model introduced by Newmark *et al*. [28] if only the in-plane bending behaviour is considered. In the Newmark's model, the geometrically linear Euler–Bernoulli beam theory (i.e. small displacements, rotations and strains) is used to model each of the two parts of the composite beam; the effects of the deformable shear connection are accounted for by using an interface model with distributed bond, and the contact between the steel and concrete components is enforced (Figure 1). The interface slip is small, since it corresponds to the difference in longitudinal displacements of the steel and composite fibres at the steel–concrete interface.

Compared to common monolithic beams, composite beams with deformable shear connection raise more challenging modelling and numerical difficulties, e.g. complex distributions of the interface slip and force can develop [29] and special measures are necessary to avoid shear-locking phenomena [30]. Despite some difficulties, three-field mixed elements [23] can be successfully adopted for numerical simulation of the behaviour of steel–concrete composite beams, producing accurate global and local results when a proper discretization of the structure is used [31].

In the present study, a 2-D steel–concrete composite frame element with deformable shear connection, previously developed by the second author [23], is used for response simulation and is augmented with the response sensitivity computation procedure presented above. The finite element used is based on the three-field mixed formulation and assumes Newmark's kinematics (Figure 1). It has 10 nodal degrees-of-freedom (DOFs) in total: eight DOFs are external, while two DOFs are internal and are condensed out before assembly at the structure level (Figure 2). The procedure for response sensitivity calculation in presence of static condensation has been previously derived by the authors and can be found elsewhere [32]. This finite element was proven to provide accurate response simulations and to be superior in the evaluation of local quantities (e.g. section

Copyright © 2006 John Wiley & Sons, Ltd.

DOI: 10.1002/nme

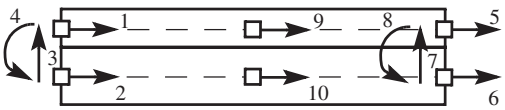

Figure 2. Degrees of freedom of the 2-D composite beam finite element.

deformations, section stress resultants, shear force distribution at the steel–concrete interface, etc.) to equivalent displacement-based finite elements when meshes requiring similar computational effort are used. Furthermore, this element presents a useful feature: it is able to model a standard monolithic steel-only or reinforced concrete-only frame element without any modification in the code. This is achieved simply by considering at the section level a concrete slab or a steel beam of null cross-section area, obtaining a monolithic steel frame or a reinforced concrete frame, respectively. The only precaution is to apply constraints to the eliminated DOFs. The obtained three-field mixed monolithic frame element is characterized by exact distributions of section stress resultants (as for force-based frame elements [19]), while the assumed displacement fields have the same form as for standard displacement-based frame elements. The above useful feature allows to assemble easily monolithic and composite frame elements in frame models, representing correctly the connections between steel columns and steel beams or reinforced concrete columns and concrete slabs [32].

Regarding the development of the sensitivity analysis, this element presents also a favourable feature: the response sensitivity computation procedure, developed for a general three-field mixed finite element and particularized to a frame element, can be further simplified significantly by taking advantage of the properties of the employed shape functions for the section deformation and section stress resultant fields. This condition derives from the fact that the shape functions used for approximating the section deformations and the section stress resultants are the same (i.e. $\mathbf{E}(x)=\mathbf{S}(x)$). This choice for the shape functions produces a matrix $\overline{\mathbf{E}}$ that is positive definite and, therefore, invertible [16]. Using this property, Equations (90) and (94) simplify to

$$\frac{\mathrm{d}\mathbf{e}(\theta)}{\mathrm{d}\theta}=\overline{\mathbf{E}}^{-1}\overline{\mathbf{B}}\frac{\mathrm{d}\mathbf{q}(\theta)}{\mathrm{d}\theta} \tag{96}$$

$$\frac{\mathrm{d}\mathbf{s}(\mathbf{e}(\theta),\theta)}{\mathrm{d}\theta}=\overline{\mathbf{E}}^{-\mathrm{T}}\frac{\mathrm{d}\mathbf{a}(\mathbf{e}(\theta),\theta)}{\mathrm{d}\theta} \tag{97}$$

In this way, inversion of the two matrices $\overline{\mathbf{D}}_t$ and $\overline{\overline{\mathbf{D}}}_t$ (required in Equations (90) and (94)) is avoided and only matrix $\overline{\mathbf{E}}$ has to be inverted. It is noteworthy that, in this special case for which $n_s=n_e$, the three matrices $\overline{\mathbf{D}}_t$, $\overline{\overline{\mathbf{D}}}_t$, and $\overline{\mathbf{E}}$ have the same dimension $n_s\times n_s=n_e\times n_e$.

4.2. Implementation of composite frame element and response sensitivity computation scheme in a general-purpose nonlinear finite element structural analysis program

For validation purposes, the steel–concrete composite frame element and the response sensitivity computation scheme for three-field mixed formulation were implemented in a general-purpose nonlinear finite element structural analysis program, FEDEASLab [33]. FEDEASLab is a Matlab toolbox [34] for linear and nonlinear, static and dynamic structural analysis, which also provides a

Copyright © 2006 John Wiley & Sons, Ltd.

DOI: 10.1002/nme

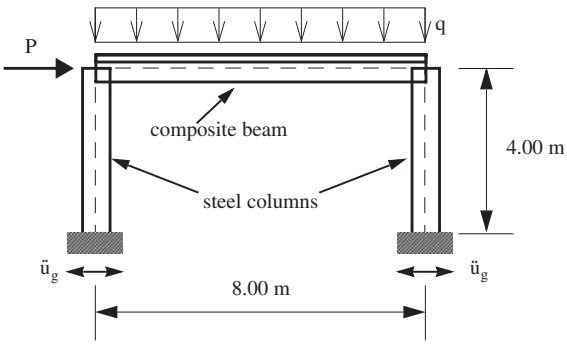

Figure 3. Steel–concrete composite frame structure.

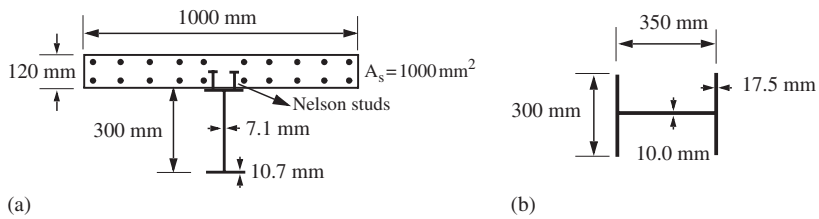

Figure 4. Cross-section properties of the steel–concrete frame structure: (a) composite beam cross-section; and (b) steel column cross-section.

general framework for parameterization of finite element models and response sensitivity computation [35].

Taking advantage of the modularity of FEDEASLab, a variety of suitable cross-sections (e.g. composite cross-section with symmetric and unsymmetric steel I-beams) and material constitutive models (e.g. Kent–Scott–Park concrete model, Popowics–Saenz concrete model with nonlinear tension stiffening) were also implemented for response and response sensitivity computation. Thus, a library of material and element models was implemented in FEDEASLab, which allows accurate response and response sensitivity analyses of steel–concrete composite frame structures. This library can be easily updated and/or extended to follow the state-of-the-art in modelling such structures.

4.3. Benchmark example: one-storey one-bay steel–concrete composite frame

The benchmark problem considered is a one-storey one-bay frame, made of two steel columns and a steel–concrete composite beam (Figure 3). The column steel section is a European HE360A; the composite beam consists of a European IPE300 steel section coupled to a reinforced concrete slab 1000 mm wide and 120 mm thick through two rows of Nelson stud connectors (Figure 4). Two identical layers of steel reinforcement with a total area $A_s = 1000\,\text{mm}^2$ are present in the slab. Two loading conditions are considered: (1) pushover analysis (after static application of a uniform distributed vertical load of 46 kN/m on the beam, representing self-weight, permanent loads and live loads, a horizontal load of increasing magnitude is applied quasi-statically at the beam–column nodes at the roof level, see Figure 3), and (2) earthquake base excitation (after

Copyright © 2006 John Wiley & Sons, Ltd.

DOI: 10.1002/nme

Table I. Material constitutive parameters.

Material	Parameter	Value	SI unit	Description
Concrete	f_c	33.0	MPa	Peak compressive strength
	E_c	32 000	MPa	Initial tangent stiffness
	ε_c	0.0022	dimensionless	Strain at peak strength
	f_f	15	MPa	Strength at inflection point
	ε_f	0.039	dimensionless	Strain at inflection point
Beam-and-column steel	f_{ys}	275	MPa	Yield strength
	E_s	210 000	MPa	Young's modulus
	$H_{kin,s}$	2100	MPa	Kinematic hardening modulus
	$H_{iso,s}$	0	MPa	Isotropic hardening modulus
	α_{0s}	0	MPa	Initial back-stress
	b_s	0.01	dimensionless	Strain hardening ratio [5]
Reinforcement steel	f_{yr}	430	MPa	Yield strength
	E_r	210 000	MPa	Young's modulus
	$H_{kin,r}$	2100	MPa	Kinematic hardening modulus
	$H_{iso,r}$	0	MPa	Isotropic hardening modulus
	α_{0r}	0	MPa	Initial back-stress
	b_r	0.01	dimensionless	Strain hardening ratio [5]
Shear connectors	f_{smax}	423	kN/m	Shear strength
	τ_{fr}	42.3	kN/m	Residual frictional stress
	δ_{ult}	6.0	mm	Slip at rupture

static application of a uniform distributed vertical load of 46 kN/m on the beam, the frame is subjected to a horizontal ground motion corresponding to the N90W (W-E) component of the Loma Prieta earthquake of 17 October 1989, recorded at the Capitola site [36], scaled by a factor 4).

The structure is discretized into six finite elements, i.e. four elements for the steel–concrete composite beam and one element for each steel column. The constitutive law used for the steel material of the beam and of the two columns as well as for the reinforcement steel is a uniaxial cyclic J_2 plasticity model with the von Mises yield criterion in conjunction with linear kinematic and isotropic hardening laws [5]. The selected constitutive law for the concrete material is a uniaxial cyclic law with monotonic envelope given by the Popovics–Saenz law [37, 38]. The constitutive law used for the shear connectors is a slip–force cyclic law with monotonic envelope given by the Ollgaard *et al*. law [39] and a cyclic response following a modified version of the model proposed by Eligenhausen *et al.* [40]. Detailed formulation and differentiation of the concrete and connection constitutive laws can be found in Reference [41]. The values of the material constitutive parameters are given in Table I. Reference [41] as well as Reference [32] also provide comparisons between analytical predictions and experimental results for the response of steel-concrete composite beams and frame structures modelled using a displacement-based frame element with deformable shear connection.

In the following, numerical simulations of important global and local response quantities as well as of their consistent sensitivities to various material parameters are presented for each of the two loading conditions defined above. In this paper, the response sensitivity results are presented in normalized form, i.e. they are multiplied by the nominal value of the sensitivity parameter and divided by a factor 100. In this way, the normalized response sensitivities represent the variation of

Copyright © 2006 John Wiley & Sons, Ltd.

DOI: 10.1002/nme

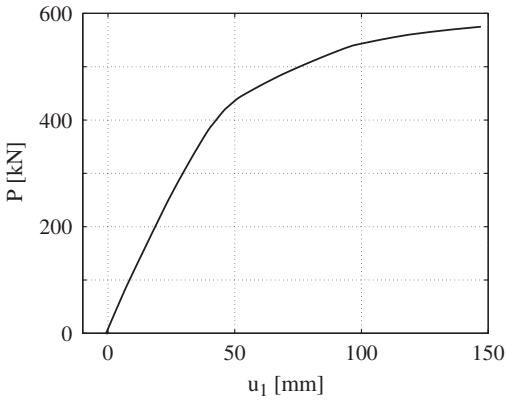

Figure 5. Pushover analysis: applied horizontal load P (total base shear) versus horizontal displacement u_1 at the left-end of the concrete slab.

the response quantity considered due to 1% change in the sensitivity parameter. These normalized sensitivities can thus be used to compare (in the deterministic sense, or considering that 1% change in the various sensitivity parameters are equally likely) the relative effects/importance of the sensitivity parameters on the response quantities considered.

4.3.1. Response and response sensitivity analysis for quasi-static load case. The quasi-static pushover analysis of the testbed structure defined above is performed using the force control method. First, a vertical distributed load $q = 46\,\text{kN/m}$ along the beam is applied statically to the structural model. Subsequently, a horizontal load P (Figure 3) of increasing magnitude is applied quasi-statically to the two horizontal DOFs of the left-end node of the composite beam, until the ultimate horizontal resisting force of the structure is reached (collapse state). The load P is equally distributed between the two DOFs (i.e. $P/2$ to each DOF), in order to simulate an equivalent earthquake loading for assumed equal tributary masses of the concrete slab and steel beam.

In Figure 5, the applied horizontal load P (representing also the total shear force at the base of the columns) is plotted versus the horizontal displacement u_1 (concrete slab DOF) of the left-end of the composite beam. Figure 6 shows the relation between the load P and the vertical displacement v at midspan of the composite beam. Figures 7 and 8plot the bending moment–curvature and shear force–slip response curves, respectively, at the left-end section of the composite beam. Figure 5 clearly shows the ductile behaviour of the considered structure that reaches a horizontal displacement u_1 of about 30 mm ($P = 300\,\text{kN}$) without a sensible stiffness degradation (almost linear behaviour at the global level, even though the local behaviour is strongly nonlinear from the beginning of the analysis, see Figure 8), while the horizontal displacement at collapse is slightly below 150 mm ($P = 575\,\text{kN}$). The change of stiffness around $u_1 = 45\,\text{mm}$ is mostly due to stiffness degradation of the composite beam, while the change of stiffness around $u_1 = 100\,\text{mm}$ ($P = 545\,\text{kN}$) is caused primarily by yielding of the columns. This is consistent with the fact that this frame structure has been designed for a 'strong column–weak beam' behaviour. In Figure 6, the changes in stiffness mentioned above can be observed even more clearly: the vertical displacement v is almost unchanged from the one produced by the vertical loads for an applied horizontal load $P = 95\,\text{kN}$, then the same stiffness changes as in Figure 5 are visible. It is noteworthy that the concrete never reaches its peak

Copyright © 2006 John Wiley & Sons, Ltd.

DOI: 10.1002/nme

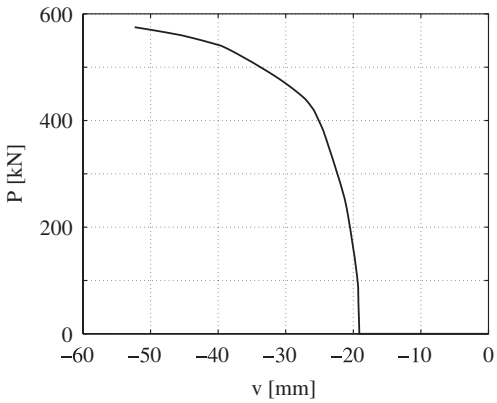

Figure 6. Pushover analysis: applied horizontal load P (total base shear) versus vertical displacement v at midspan of the composite beam.

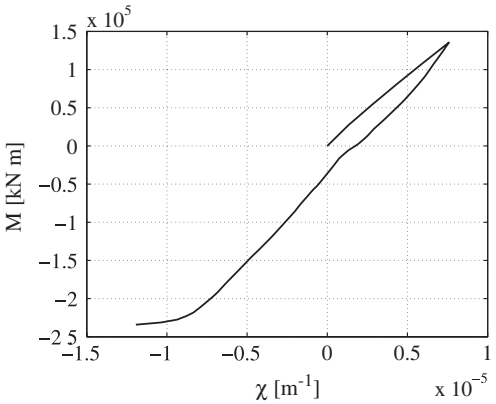

Figure 7. Pushover analysis: moment–curvature response at the left-end section of the composite beam.

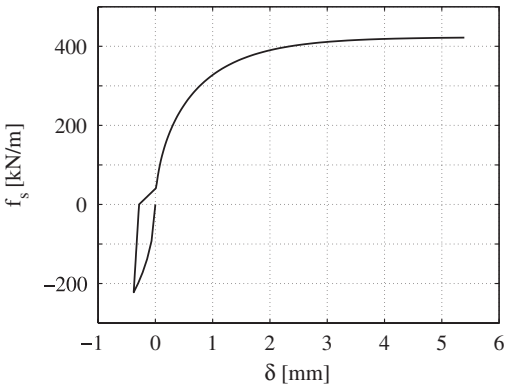

Figure 8. Pushover analysis: shear force–slip response at the left-end section of the composite beam.

Copyright © 2006 John Wiley & Sons, Ltd.

DOI: 10.1002/nme

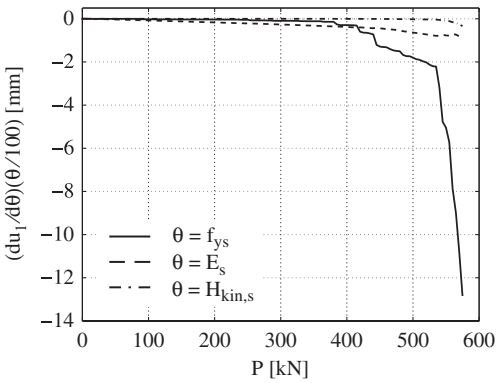

Figure 9. Pushover analysis: sensitivities of horizontal displacement u_1 to beam-and-column steel material parameters.

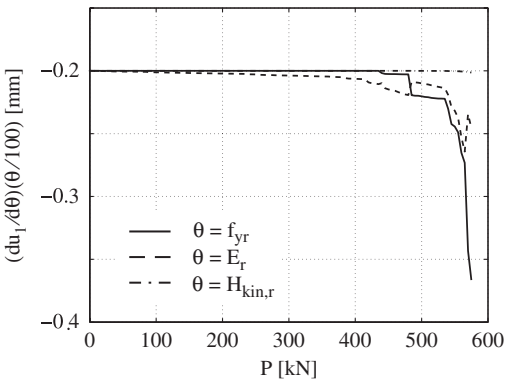

Figure 10. Pushover analysis: sensitivities of horizontal displacement u_1 to reinforcement steel material parameters.

compressive strength and the shear connectors do not fail before the entire structure reaches the collapse state (structure tangent stiffness matrix nearly singular). The moment and shear force at the left-end section of the composite beam change sign (compared with their values after application of the gravity loads) during the pushover, as shown in Figures 7 and 8, respectively. In Figure 8, a phase of reduced stiffness (pinching) is observed in the shear force-slip behaviour. This stiffness reduction in the shear connection behaviour models the closing of voids/gaps and cracks due to the inversion of the shear force.

Figures 9–28 present sensitivity results for the pushover analysis of the frame structure regarding the global (u_1 and v) and local (M and f_s) response quantities defined previously. Figures 9–12 plot the response sensitivities of the horizontal displacement u_1 to material parameters of the steel material of the beam and columns, the reinforcement steel, the concrete and the shear connection, respectively. Figure 13 shows a direct comparison of the sensitivities of the horizontal displacement u_1 to the strength parameters of the steel of the beam and columns (f_{ys}), the concrete (f_c) and the shear connection (f_{smax}). From these figures, it is observed that the response quantity

Copyright © 2006 John Wiley & Sons, Ltd.

DOI: 10.1002/nme

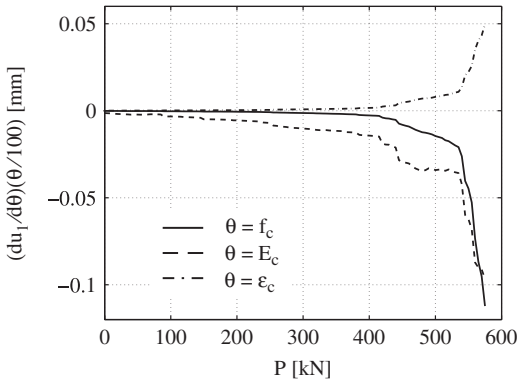

Figure 11. Pushover analysis: sensitivities of horizontal displacement u_1 to concrete material parameters.

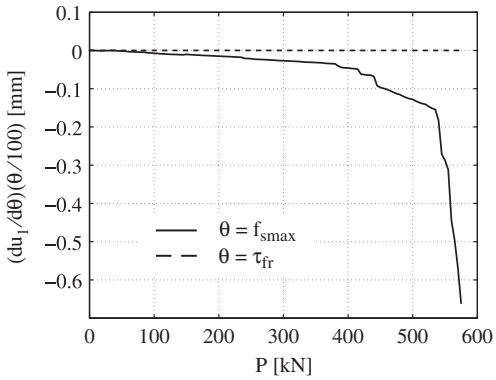

Figure 12. Pushover analysis: sensitivities of horizontal displacement u_1 to shear connection material parameters.

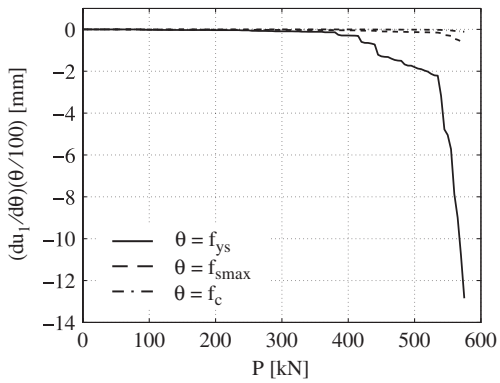

Figure 13. Pushover analysis: sensitivities of horizontal displacement u_1 to strength parameters of beam-and-column steel, concrete and shear connection.

Copyright © 2006 John Wiley & Sons, Ltd.

DOI: 10.1002/nme

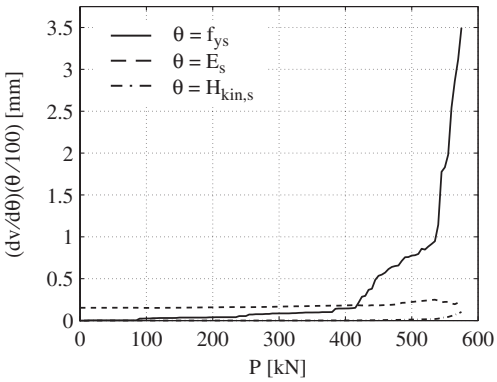

Figure 14. Pushover analysis: sensitivities of vertical displacement v at midspan of the composite beam to beam-and-column steel material parameters.

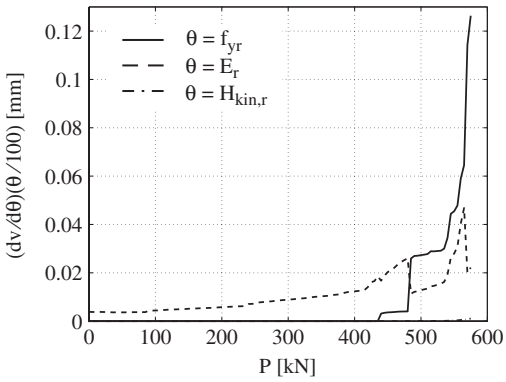

Figure 15. Pushover analysis: sensitivities of vertical displacement v at midspan of the composite beam to reinforcement steel material parameters.

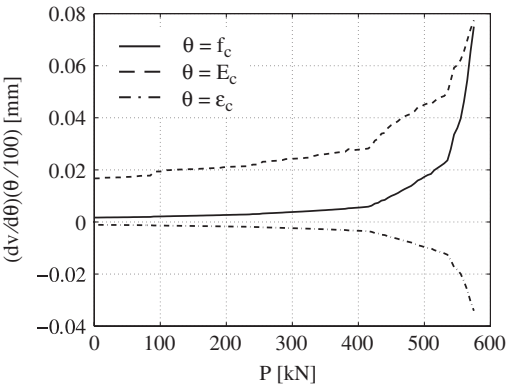

Figure 16. Pushover analysis: sensitivities of vertical displacement v at midspan of the composite beam to concrete material parameters.

Copyright © 2006 John Wiley & Sons, Ltd.

DOI: 10.1002/nme

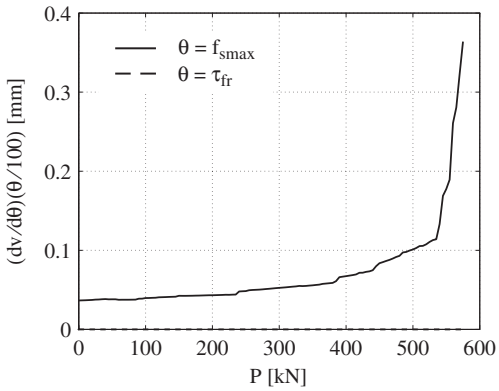

Figure 17. Pushover analysis: sensitivities of vertical displacement v at midspan of the composite beam to shear connection material parameters.

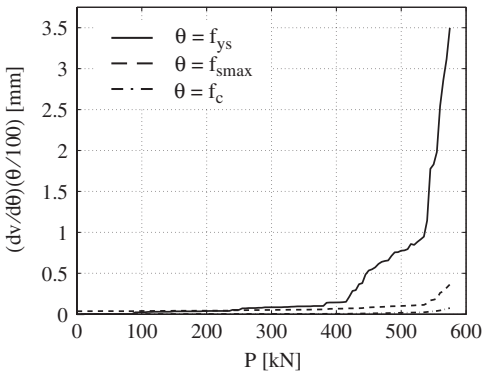

Figure 18. Pushover analysis: sensitivities of vertical displacement v at midspan of the composite beam to strength parameters of beam-and-column steel, concrete and shear connection materials.

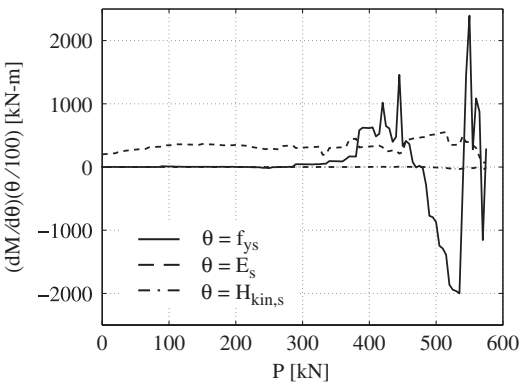

Figure 19. Pushover analysis: sensitivities of bending moment M acting at the left-end composite beam section to beam-and-column steel material parameters.

Copyright © 2006 John Wiley & Sons, Ltd.

DOI: 10.1002/nme

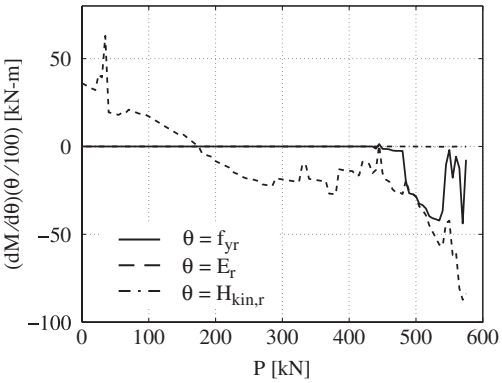

Figure 20. Pushover analysis: sensitivities of bending moment M acting at the left-end composite beam section to reinforcement steel material parameters.

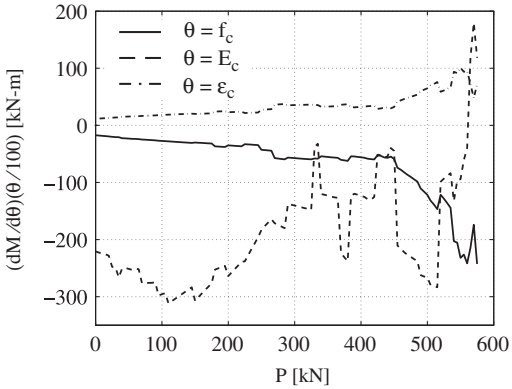

Figure 21. Pushover analysis: sensitivities of bending moment M acting at the left-end composite beam section to concrete material parameters.

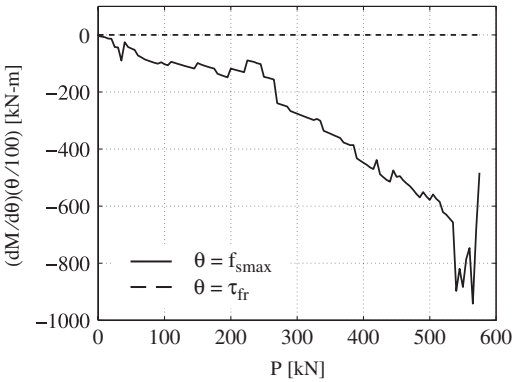

Figure 22. Pushover analysis: sensitivities of bending moment M acting at the left-end composite beam section to shear connection material parameters.

Copyright © 2006 John Wiley & Sons, Ltd.

DOI: 10.1002/nme

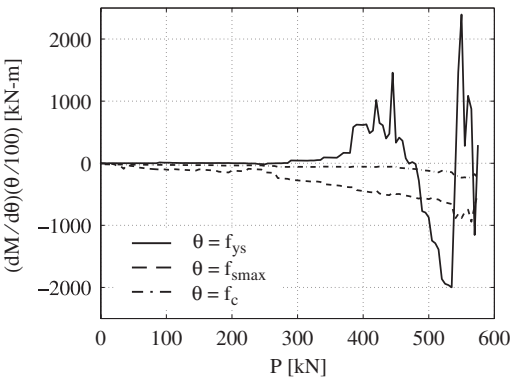

Figure 23. Pushover analysis: sensitivities of bending moment M acting at the left-end composite beam section to strength parameters of beam-and-column steel, concrete and shear connection materials.

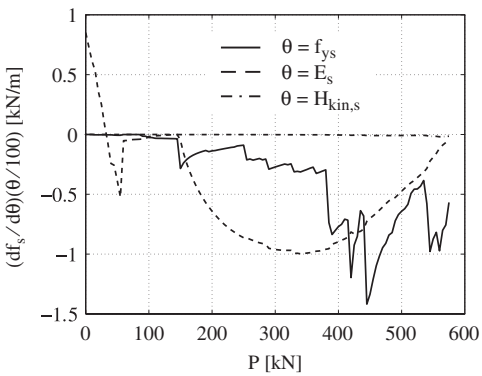

Figure 24. Pushover analysis: sensitivities of connection shear force f_s acting at the left-end composite beam section to beam-and-column steel material parameters.

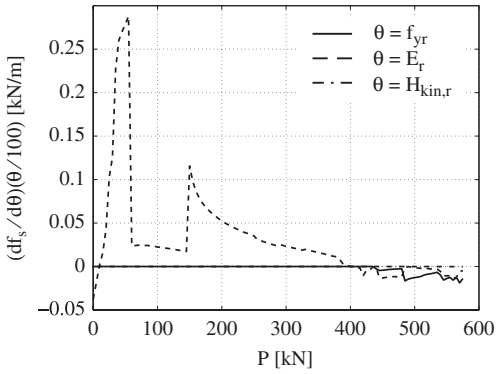

Figure 25. Pushover analysis: sensitivities of connection shear force f_s acting at the left-end composite beam section to reinforcement steel material parameters.

Copyright © 2006 John Wiley & Sons, Ltd.

DOI: 10.1002/nme

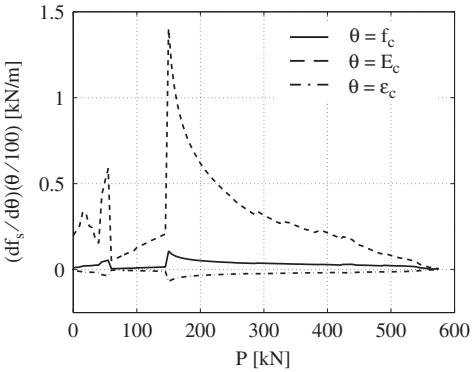

Figure 26. Pushover analysis: sensitivities of connection shear force f_s acting at the left-end composite beam section to concrete material parameters.

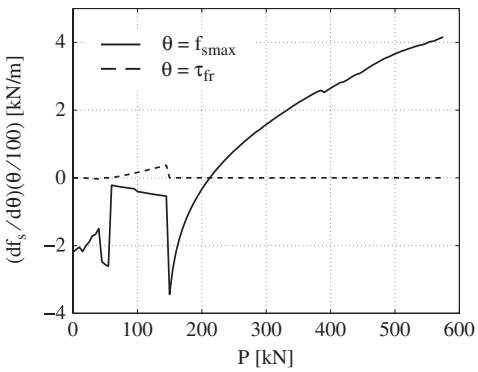

Figure 27. Pushover analysis: sensitivities of connection shear force f_s acting at the left-end composite beam section to shear connection material parameters.

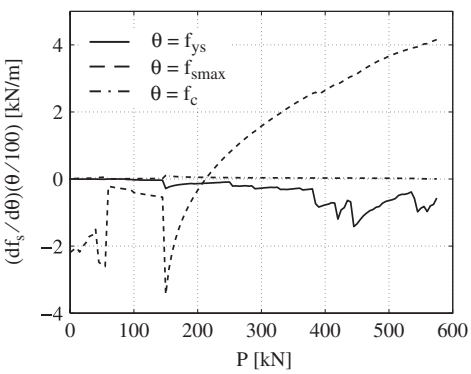

Figure 28. Pushover analysis: sensitivities of connection shear force f_s acting at the left-end composite beam section to strength parameters of beam-and-column steel, concrete and shear connection materials.

Copyright © 2006 John Wiley & Sons, Ltd.

DOI: 10.1002/nme

u_1 is more sensitive to material stiffness parameters (E_s, E_r, E_c) in the first phase of the analysis (in which the global behaviour of the structure is almost linear), but becomes dominantly sensitive to strength parameters (f_{ys}, f_{yr}, f_c, f_{smax}) when the structure approaches its collapse state. It can be seen that f_{ys} is the material parameter affecting the most the response quantity u_1, especially near the collapse load. Similarly, the response sensitivities to material parameters of the beam-and-column steel material, the reinforcement steel, the concrete and the shear connection are displayed in Figures 14–17 for the vertical displacement v, in Figures 19–22 for the bending moment M acting at the left-end composite beam section and in Figures 24–27 for the shear force f_s acting at the left-end composite beam section, respectively. Figures 18, 23 and 28 compare the sensitivities to material strength parameters f_{ys}, f_c and f_{smax} of the vertical displacement v, the bending moment M and the shear force f_s, respectively. Among the material parameters considered, the parameter that affects the most the vertical displacement v and the bending moment M is the yield strength f_{ys} of the beam-and-column steel material, while the shear force f_s is most affected by the shear strength f_{smax} of the shear connection.

In addition, the above stand-alone sensitivity results allow the following considerations, useful for gaining insight into the nonlinear response behaviour of the considered structure to quasi-static pushover:

(a) Parameters ε_f and f_f, describing the degrading branch of the concrete constitutive law, do not affect the response behaviour of the considered frame. In fact, the concrete never reaches its peak strength and therefore the response sensitivities with respect to ε_f and f_f are equal to zero for the entire pushover analysis. For this reason, these sensitivities are not plotted in Figures 11, 16, 21 and 26.
(b) Parameter τ_{fr} (residual frictional stress per unit length of the shear connection [32]) does not affect sensibly the response quantities considered (see Figures 12, 17, 22 and 27), consistently with the fact that the shear connection does not reach failure (residual frictional state).
(c) Stiffness-related material parameters significantly affect the response at low loading levels, while strength-related material parameters become predominant at high loading levels, particularly near failure (see in particular Figures 14–16). Sensitivity analysis not only confirms this intuitive result, but also allows to precisely quantify the effects and relative importance of the different material parameters at different loading stages.

Figures 29–31 present the results of a convergence study of the sensitivities of the horizontal displacement u_1 computed through the forward FDM (using increasingly small $\Delta\theta/\theta$ ratio) to the sensitivity results obtained using the DDM, for material parameters f_{ys}, f_c and f_{smax}, respectively. Results of the same convergence study are shown in Figures 32–34 for sensitivities of the connection shear force f_s acting at the left-end composite beam section to the same material parameters f_{ys}, f_c and f_{smax}. The insets in Figures 29–34 show zoom views that allow to better appreciate the convergence trends. In these figures, the results corresponding to three different values of parameter perturbation (i.e. 10^{-1}, 10^{-2} and 10^{-5} of the nominal value of the considered parameter) are plotted together with the exact DDM sensitivities. These values of the $\Delta\theta/\theta$ ratio have been carefully selected in order to obtain a clear visual display of the convergence trends, and particular attention has been given in choosing the lower value of parameter perturbation so as to avoid numerical problems related to round-off errors ('step-size dilemma', see References [5, 6, 8, 32, 42]). Convergence studies for other response quantities and other material parameters have also been performed, giving similar results in terms of convergence of forward FDM computations to DDM sensitivities for decreasing parameter perturbation

Copyright © 2006 John Wiley & Sons, Ltd.

DOI: 10.1002/nme

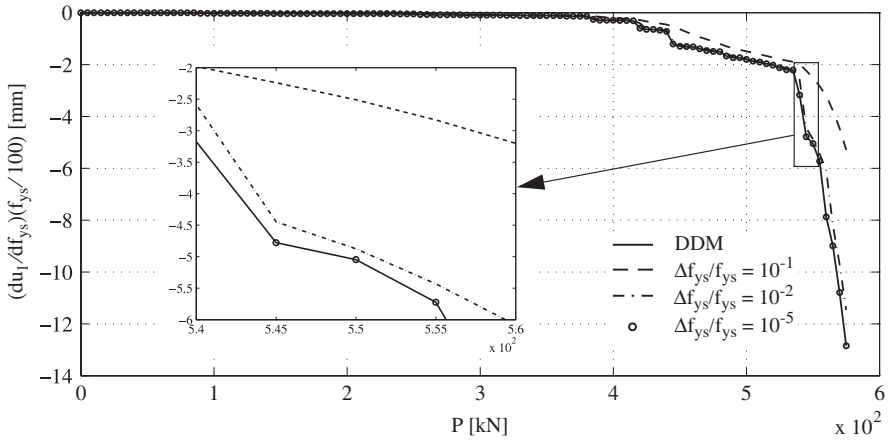

Figure 29. Convergence study of forward FDM to DDM sensitivity results for pushover analysis: sensitivities of horizontal displacement u_1 to yielding strength f_{ys} of beam-and-column steel material.

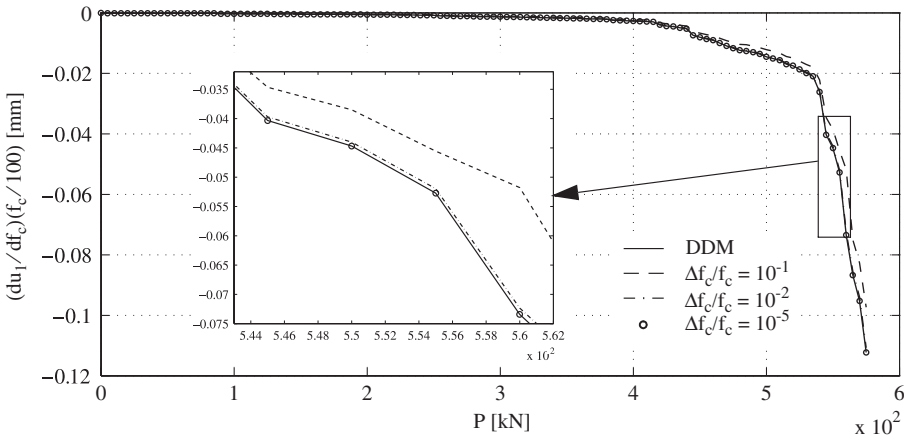

Figure 30. Convergence study of forward FDM to DDM sensitivity results for pushover analysis: sensitivities of horizontal displacement u_1 to peak strength f_c of concrete material.

values [41]. These convergence results validate the DDM-based algorithms for response sensitivity computation presented in this paper and their computer implementation for finite elements based on the three-field mixed formulation in the case of quasi-static structural analysis.

4.3.2. Response and response sensitivity analysis for dynamic load case. In dynamic analysis, the inertia and damping properties of the structure must also be included in the model. The total mass of the frame has been discretized into translational (horizontal and vertical) masses lumped at the two external nodes of each composite beam element. The mass corresponding to the permanent and live loads (i.e. total vertical distributed load of 40 kN/m) was distributed evenly between the slab and

Copyright © 2006 John Wiley & Sons, Ltd.

DOI: 10.1002/nme

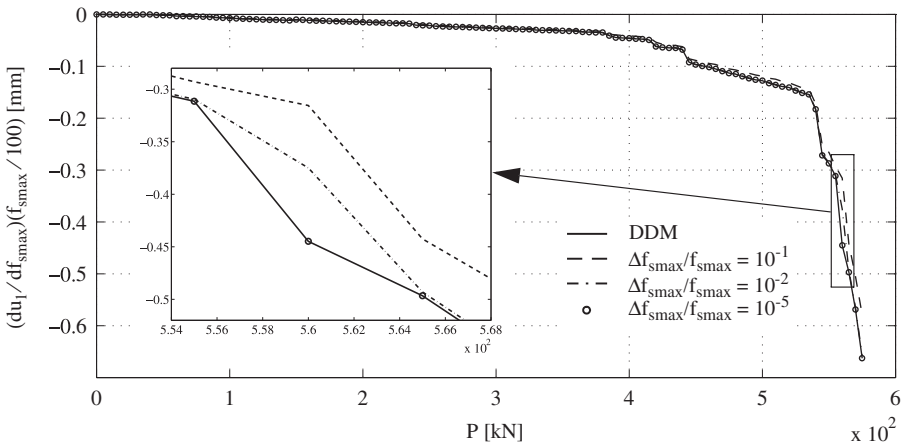

Figure 31. Convergence study of forward FDM to DDM sensitivity results for pushover analysis: sensitivities of horizontal displacement u_1 to shear strength f_{smax} of shear connection material.

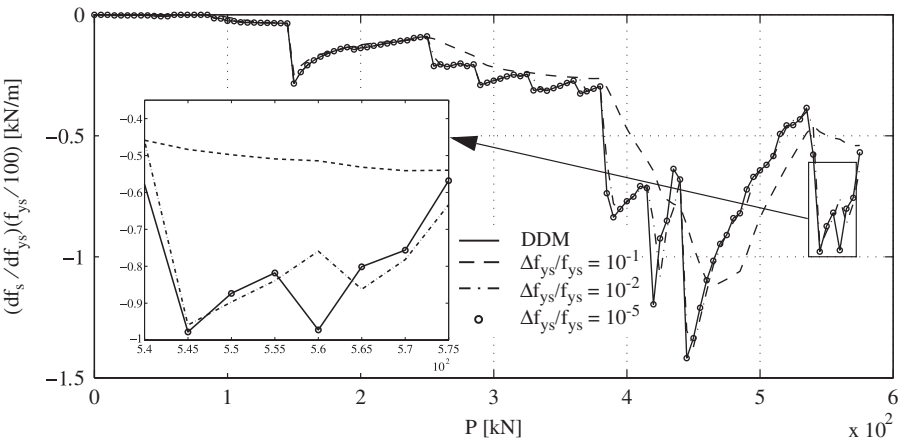

Figure 32. Convergence study of forward FDM to DDM sensitivity results for pushover analysis: sensitivities of connection shear force f_s acting at the left-end composite beam section to yield strength f_{ys} of beam-and-column steel material.

steel beam and added to the self-weight (5 kN/m for the slab and 1 kN/m for the beam). Half of the mass corresponding to the self-weight of the columns was added to the DOFs at the nodes where steel beam and column are connected. With this assumed distribution of masses, an eigenanalysis was performed using the initial stiffness properties of the structure. The first vibration mode of period $T_1 = 0.30$ s corresponds to a horizontal translation of the entire composite beam, while the second and third modes of vibration of period $T_2 = 0.18$ s and $T_3 = 0.13$ s, respectively, correspond to vertical motions. The other modes of vibration correspond to axial compression-tension modes in the composite beams and vertical modes of the frame; they are all characterized by short periods

Copyright © 2006 John Wiley & Sons, Ltd.

DOI: 10.1002/nme

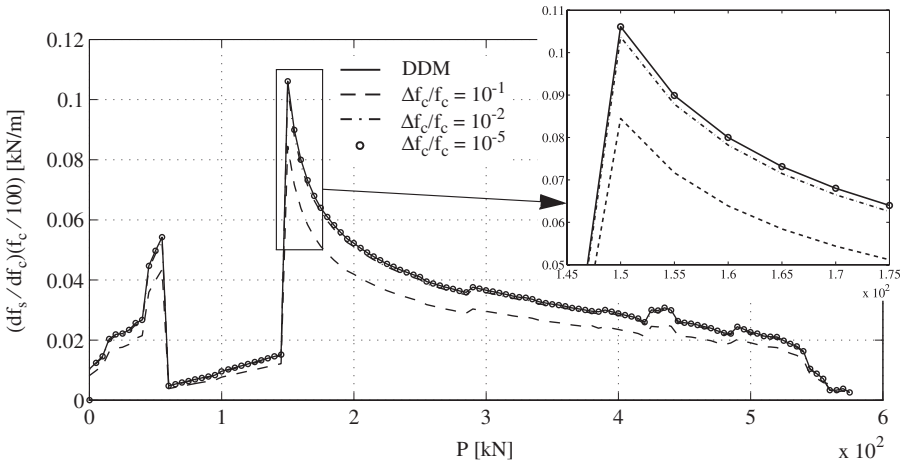

Figure 33. Convergence study of forward FDM to DDM sensitivity results for pushover analysis: sensitivities of connection shear force f_s acting at the left-end composite beam section to peak strength f_c of concrete material.

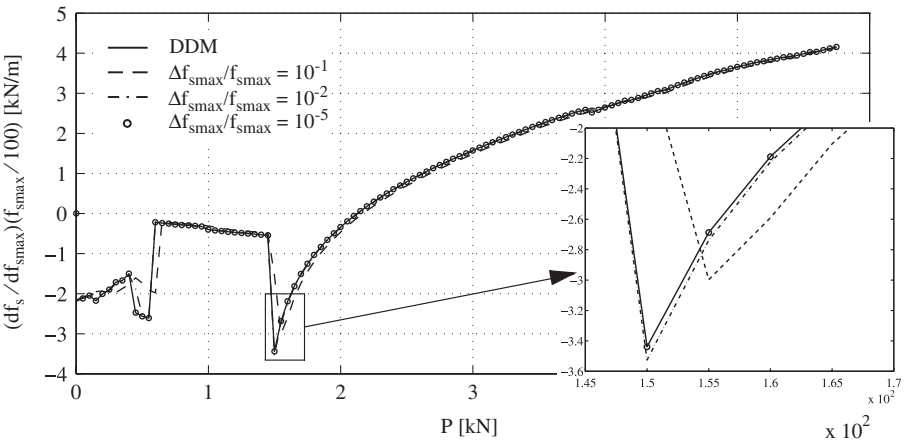

Figure 34. Convergence study of forward FDM to DDM sensitivity results for pushover analysis: sensitivities of connection shear force f_s acting at the left-end composite beam section to shear strength f_{smax} of shear connection material.

and small modal participating masses. From the modal analysis results, a Rayleigh-type damping matrix [43], proportional to the time-invariant mass and initial stiffness matrices, was computed based on an assumed damping ratio $\xi = 0.05$ for the first and third modes.

After static application of a vertical distributed load of 46 kN/m along the beam, the frame is subjected to a horizontal seismic motion corresponding to the first 30 s of the N90W (W-E) component of the Loma Prieta earthquake of 17 October 1989, recorded at the Capitola site [36],

Copyright © 2006 John Wiley & Sons, Ltd.

DOI: 10.1002/nme

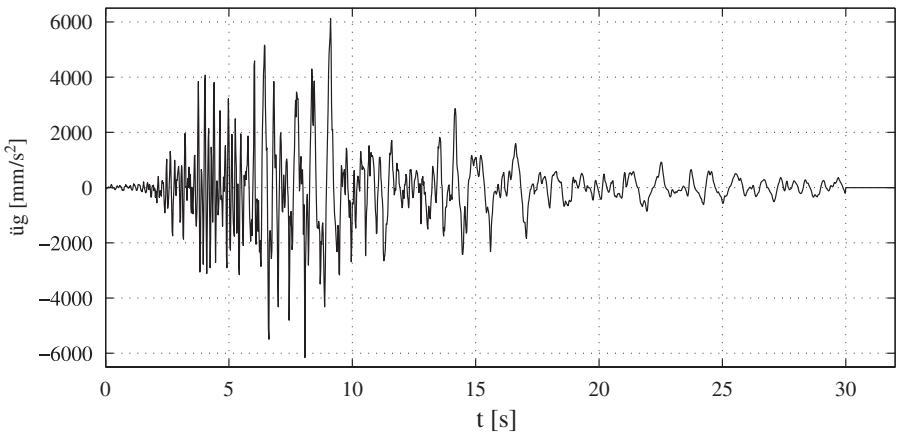

Figure 35. N90W (W-E) component of the Loma Prieta earthquake of 17 October 1989, recorded at the Capitola site, scaled by a factor of four.

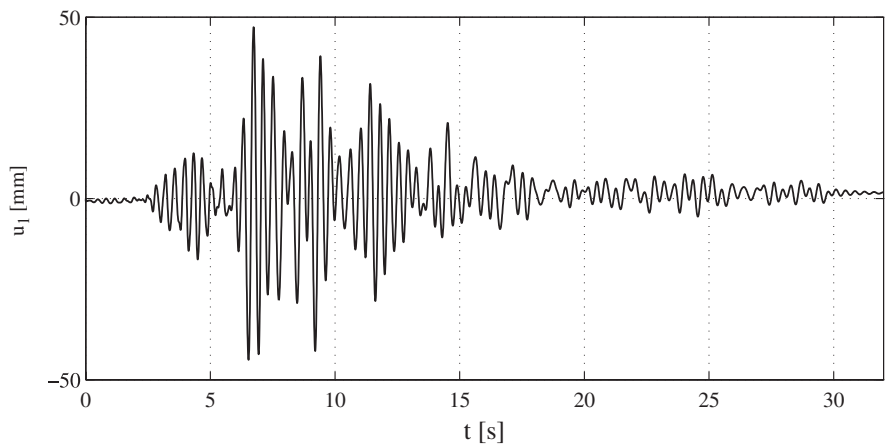

Figure 36. Dynamic analysis: horizontal displacement u_1 response history.

scaled by a factor of four to yield a peak ground acceleration of $6160\,\mathrm{mm/s^2}$ or $0.62g$ (see Figure 35), and with 2 s of zero ground motion acceleration added at the end of the record in order to capture the free-vibration properties of the structure with yielded/degraded material properties at the end of the earthquake. The equation of motion and response sensitivity equation are integrated using the constant-average-acceleration method [43] with a constant time step of $\Delta t = 0.005\,\mathrm{s}$. The following figures present results of the response history analysis performed.

Figures 36 and 37show the time histories of the horizontal displacement u_1 and vertical displacement v, respectively. The moment–curvature response at the left-end composite beam section is plotted in Figure 38, while the shear force–slip response at the same section is given in Figure 39. During the earthquake ground motion, extensive plastic behaviour is developed by the structure. In particular, the vertical displacement v exhibits a large increase due to inelastic defor-

Copyright © 2006 John Wiley & Sons, Ltd.

DOI: 10.1002/nme

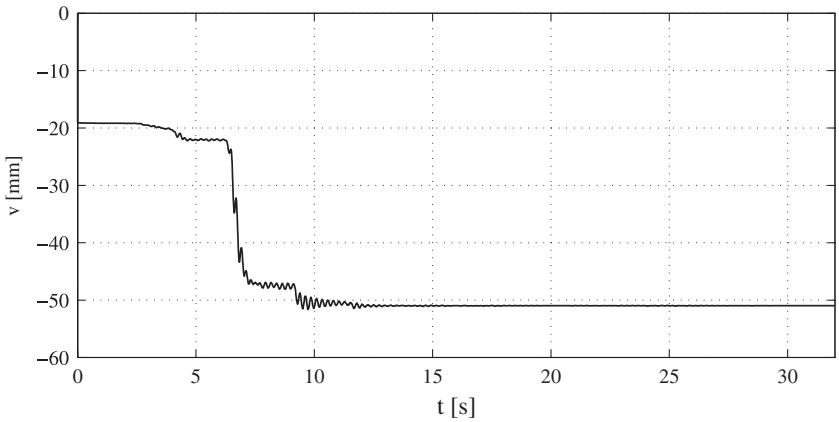

Figure 37. Dynamic analysis: vertical displacement v response history.

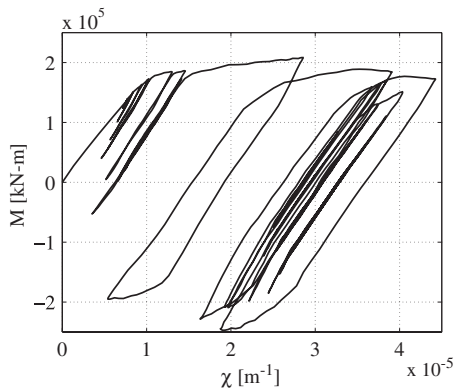

Figure 38. Dynamic analysis: moment–curvature response at the left-end section of the composite beam.

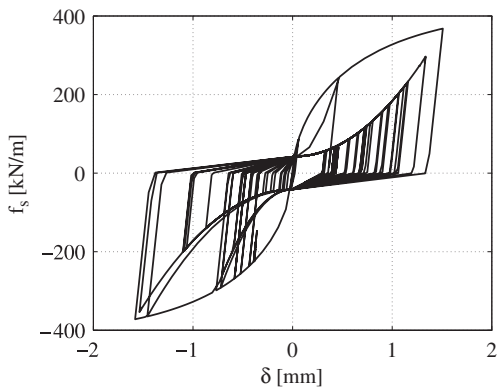

Figure 39. Dynamic analysis: shear force–slip response at the left-end section of the composite beam.

Copyright © 2006 John Wiley & Sons, Ltd.

DOI: 10.1002/nme

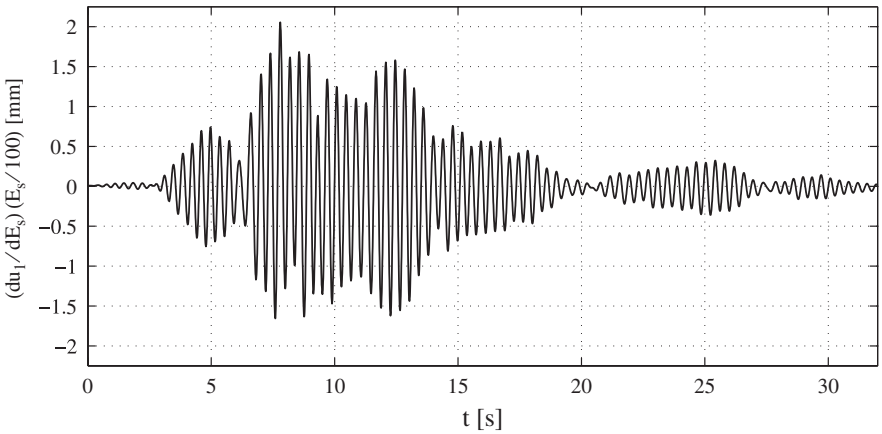

Figure 40. Dynamic analysis: sensitivity of horizontal displacement u_1 to Young's modulus E_s of the beam-and-column steel material.

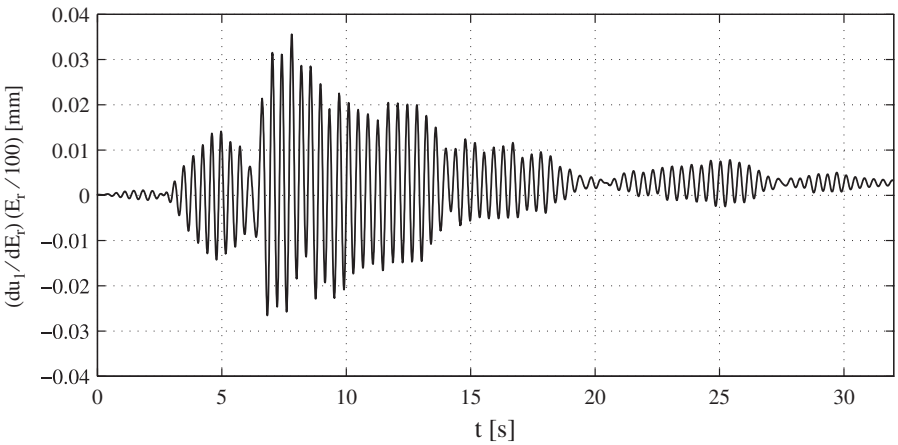

Figure 41. Dynamic analysis: sensitivity of horizontal displacement u_1 to Young's modulus E_r of reinforcement steel material.

mation at around $t = 7$ s (Figure 37) and the hysteretic behaviour of the shear force–slip response is pronounced (Figure 39). From Figure 36, it can be seen that the maximum horizontal displacement (47 mm) is moderately large (corresponding to an interstory drift ratio of 1.2%) and the frame exhibits a small permanent horizontal deformation at the end of the earthquake. While the moment–curvature response at the section level (Figure 38) remains quasi-linear during application of the gravity loads, the hysteretic behaviour is significant during the earthquake response including some degradation of the flexural capacity. The curvature ductility (defined as ratio between the maximum curvature and the curvature at yielding) is about five (see Figure 38). It is noteworthy that the structural performance of the present benchmark steel-concrete composite frame, when subjected to the earthquake excitation considered, is satisfactory since the plastic behaviour is limited to the beam,

Copyright © 2006 John Wiley & Sons, Ltd.

DOI: 10.1002/nme

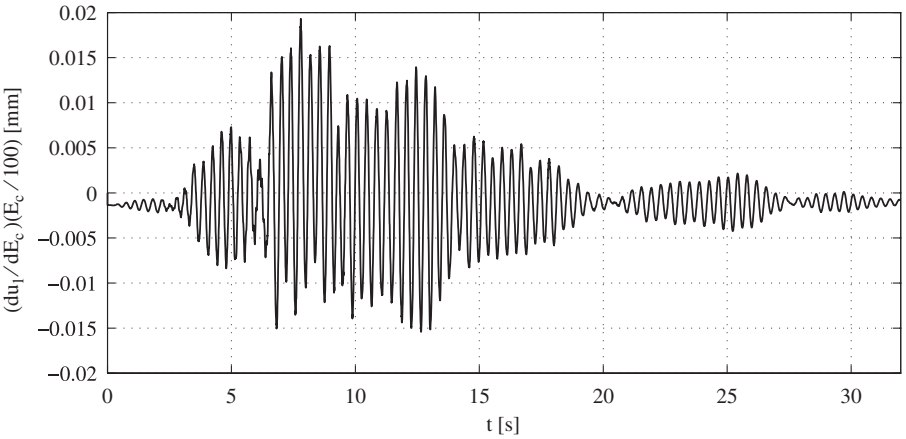

Figure 42. Dynamic analysis: sensitivity of horizontal displacement u_1 to initial tangent stiffness E_c of concrete material.

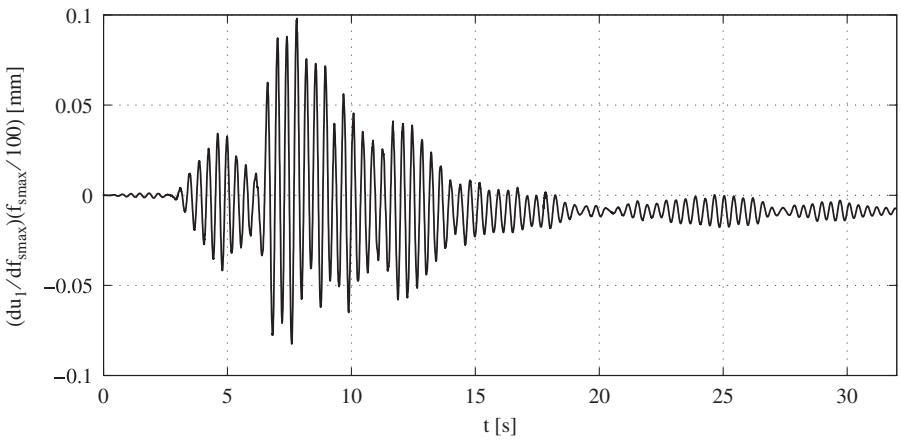

Figure 43. Dynamic analysis: sensitivity of horizontal displacement u_1 to shear strength f_{smax} of shear connection material.

the permanent deformations are small and brittle failure mechanisms (such as concrete crushing and rupture of the shear connection) are avoided.

Figures 40–43 show the normalized sensitivities of the horizontal displacement u_1 to Young's modulus E_s of the beam-and-column steel, Young's modulus E_r of the reinforcement steel, the initial tangent stiffness E_c of concrete, and the strength f_{smax} of the shear connection, respectively. The choice of plotting these sensitivities is driven by the fact that, for the dynamic case, material stiffness related parameters affect the horizontal displacement u_1 more than strength related parameters. This is shown in Figure 44, which compares the sensitivities of the horizontal displacement u_1 to the material parameters affecting the most this response quantity. The response sensitivity histories are observed to have similar waveforms (frequency content) to that of the time history of u_1 and exhibit a small shift in their mean value. This feature is linked to the material constitutive laws

Copyright © 2006 John Wiley & Sons, Ltd.

DOI: 10.1002/nme

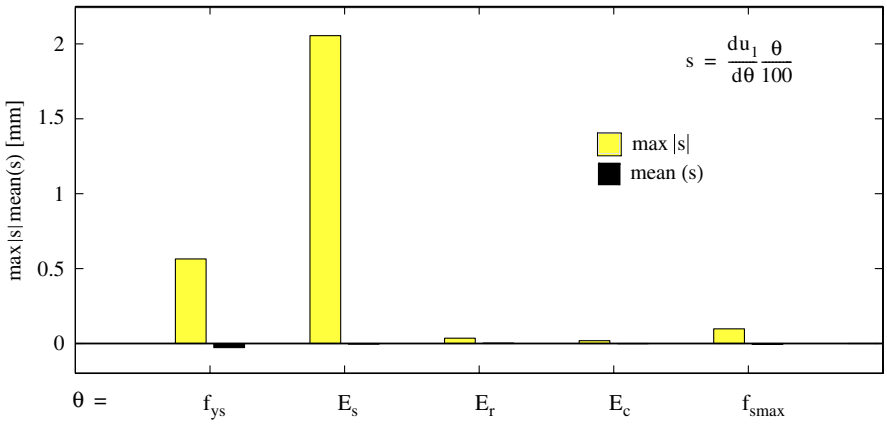

Figure 44. Dynamic analysis: comparison of sensitivities of horizontal displacement u_1 to material parameters to which u_1 is most sensitive.

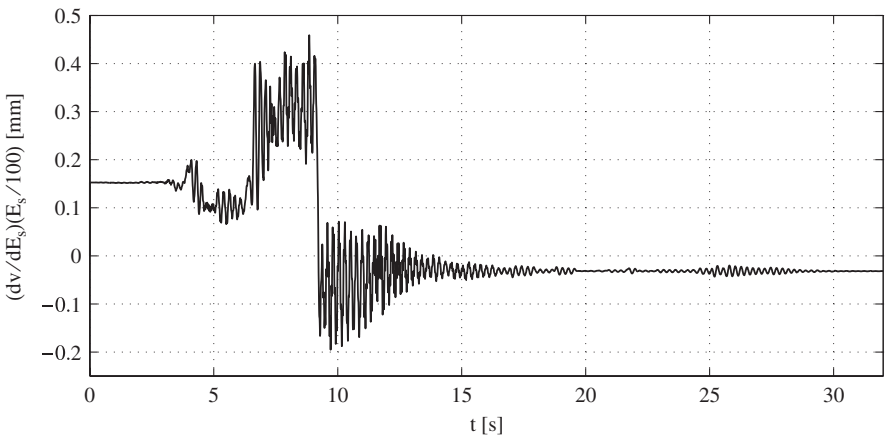

Figure 45. Dynamic analysis: sensitivity of vertical displacement v at midspan of composite beam to Young's modulus E_s of the beam-and-column steel material.

employed: all these constitutive laws (except for the concrete constitutive model beyond the peak strength, which was not reached in the dynamic load case presented here) use the initial tangent stiffness for unloading from plastic branches, and thus the effective first period of vibration of the structure remains close to the initial fundamental period even after large plastic deformations are experienced by the structure (waveform similarity). The small shift in mean value of the response sensitivities is due to the hysteretic nature of the material constitutive laws.

Figure 45 shows the sensitivity of the vertical displacement v at midspan of the composite beam to Young's modulus E_s of the beam-and-column steel material, while Figure 46 compares the sensitivities of v to the material parameters to which this response quantity is most

Copyright © 2006 John Wiley & Sons, Ltd.

DOI: 10.1002/nme

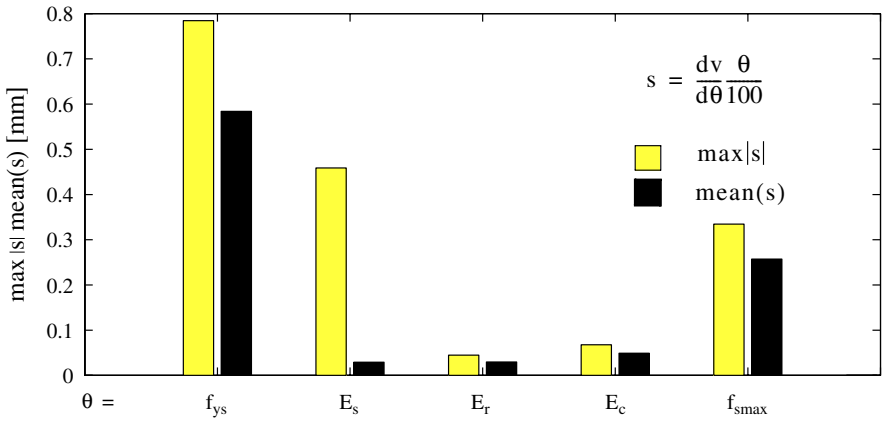

Figure 46. Dynamic analysis: comparison of sensitivities of vertical displacement v to material parameters to which v is most sensitive.

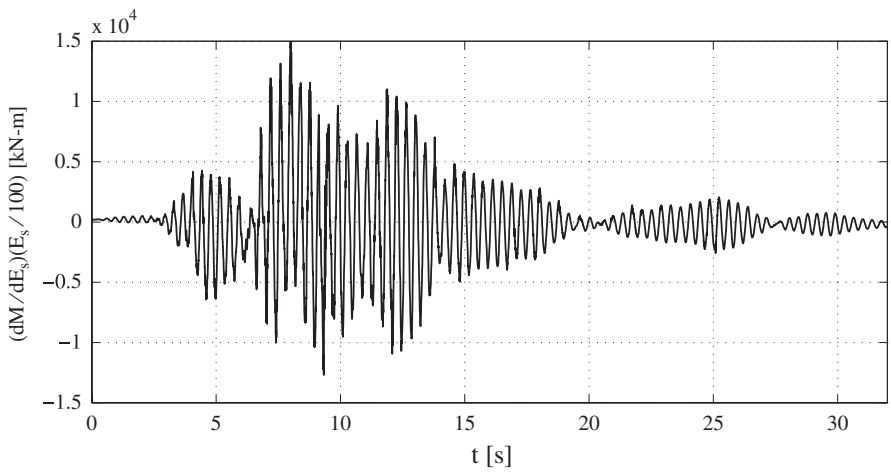

Figure 47. Dynamic analysis: sensitivity of bending moment M acting at the left-end section of the composite beam to Young's modulus E_s of the beam-and-column steel material.

sensitive. Similarly, Figure 47 shows the sensitivity of the bending moment M acting at the left-end composite beam section to Young's modulus E_s of the beam-and-column steel material and Figure 48 compares the sensitivities of M to material parameters to which M is most sensitive. Figure 49 shows the sensitivity of the shear force f_s acting at the left-end composite beam section to Young's modulus E_s of the beam-and-column steel material, while Figure 50 compares the sensitivities of f_s to material parameters to which f_s is most sensitive. The material parameter affecting the most the bending moment M and the shear force f_s is Young's modulus E_s of the beam-and-column steel material, while the material parameter to which the vertical

Copyright © 2006 John Wiley & Sons, Ltd.

DOI: 10.1002/nme

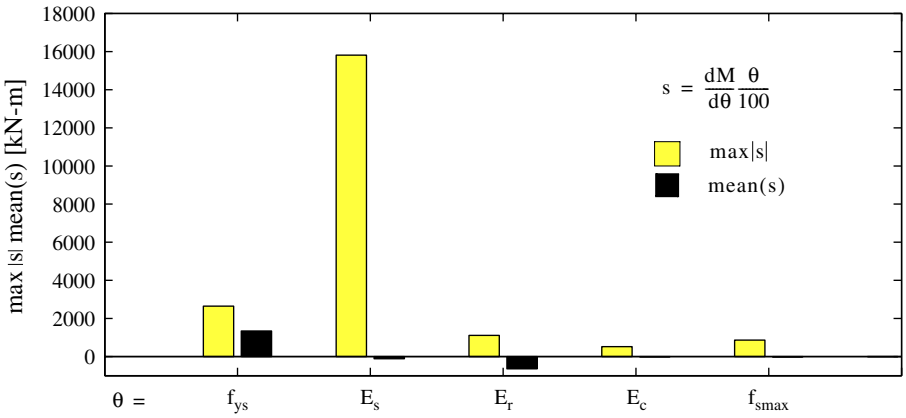

Figure 48. Dynamic analysis: comparison of sensitivities of bending moment M acting at the left-end composite beam section to material parameters to which M is most sensitive.

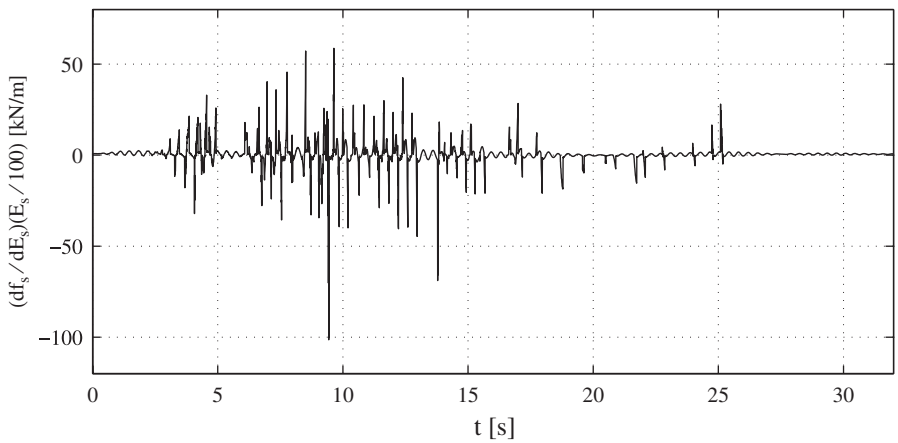

Figure 49. Dynamic analysis: sensitivity of connection shear force f_s acting at the left-end section of the composite beam to Young's modulus E_s of the beam-and-column steel material.

displacement v is most sensitive is the yield strength f_{ys} of the beam-and-column steel material. The dynamic response sensitivity analysis shows that the global and local responses of the considered structure are most sensitive to the material parameters describing the constitutive law of the beam-and-column steel material, as was already the case for the pushover loading and as expected from design considerations.

Figure 51 shows the sensitivities of the vertical displacement v to the yield strength f_{ys} of the beam-and-column steel material computed using both DDM and forward FDM for decreasing values of the parameter perturbation. Figure 52 shows a closer view of the convergence of the forward FDM results to the DDM results. Similarly, the sensitivities of the bending

Copyright © 2006 John Wiley & Sons, Ltd.

DOI: 10.1002/nme

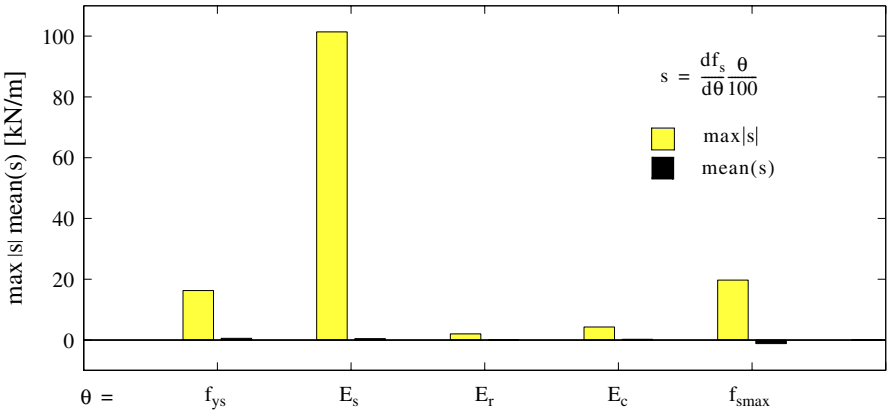

Figure 50. Dynamic analysis: comparison of response sensitivities of connection shear force f_s acting at the left-end composite beam section to material parameters to which f_s is most sensitive.

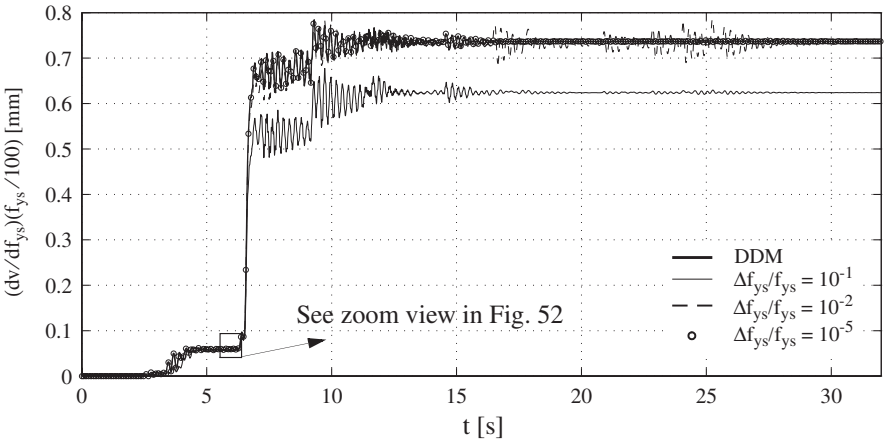

Figure 51. Convergence study of forward FDM to DDM sensitivity results for dynamic analysis: sensitivity of vertical displacement v at midspan of composite beam to yield strength f_{ys} of the beam-and-column steel material.

moment M to the yield strength f_{ys}, computed via the forward FDM for decreasing values of the parameter perturbation are plotted in Figure 53 together with the corresponding response sensitivity computed using the DDM. Figure 54 offers a zoom view of the previous figure, showing again convergence of the forward FDM results to the DDM results. These results, together with the results of other convergence studies (not shown here) performed by the authors for the sensitivities of other response quantities to all the material parameters considered in this paper, validate the DDM-based algorithms for response sensitivity computation presented in this paper and their computer implementation for finite elements based on the three-field mixed formulation in the cases of quasi-static and dynamic structural analysis.

Copyright © 2006 John Wiley & Sons, Ltd.

DOI: 10.1002/nme

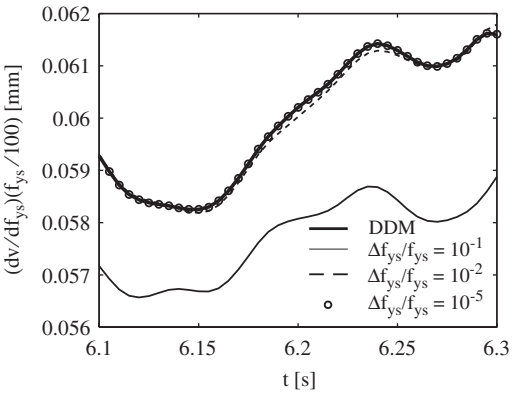

Figure 52. Convergence study of forward FDM to DDM sensitivity results for dynamic analysis: zoom view of sensitivity of vertical displacement v at midspan of composite beam to yield strength f_{ys} of the beam-and-column steel material (see Figure 51).

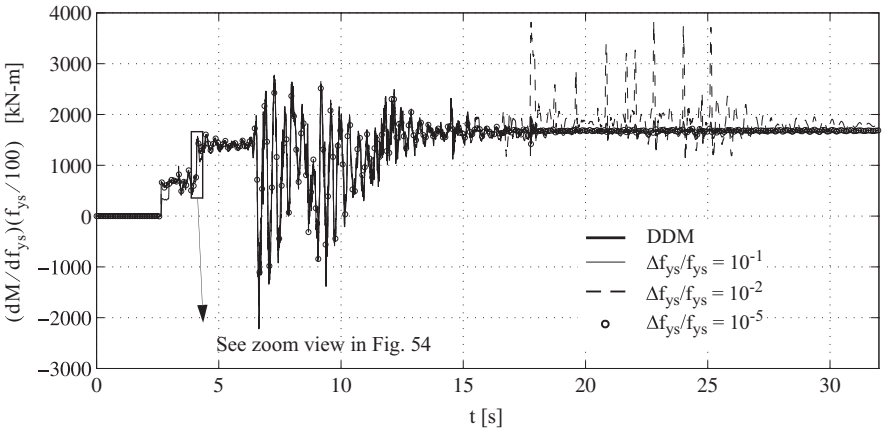

Figure 53. Convergence study of forward FDM to DDM sensitivity results for dynamic analysis: sensitivity of bending moment M acting at the left-end composite beam section to yield strength f_{ys} of beam-and-column steel material.

5. CONCLUSIONS

This paper presents a newly developed response sensitivity computation methodology for nonlinear finite element based on a three-field mixed formulation derived from the Hu–Washizu functional. The formulation developed is based on the general DDM, which consists of differentiating consistently the space (finite element) and time (finite difference) discrete equations of the structural response. The response sensitivity computation algorithm for three-field mixed finite element formulation is presented for the general case of geometric and material nonlinearities considering response sensitivity to geometric, material and loading parameters. This general algorithm is then specialized for materially only nonlinear finite element models (i.e. linear

Copyright © 2006 John Wiley & Sons, Ltd.

DOI: 10.1002/nme

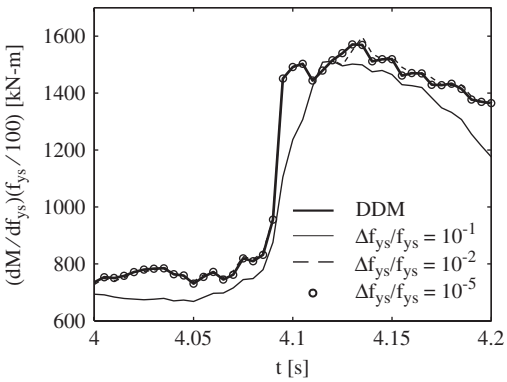

Figure 54. Convergence study of forward FDM to DDM sensitivity computations for dynamic analysis: zoom view sensitivity of bending moment M acting at the left-end composite beam section to yield strength f_{ys} of beam-and-column steel material (see Figure 53).

geometry) and is presented in detail for 2-D frame finite elements. Particular attention is given to steel–concrete composite frame finite elements, for which the three-field mixed formulation has been found beneficial in terms of accuracy in the numerical results. The DDM sensitivity computations are validated by comparisons with the forward FDM using as application example a realistic steel–concrete composite frame under quasi-static and dynamic loading. The finite element model of the proposed benchmark structure includes both monolithic beam elements and composite beam elements with deformable shear connection based on the three-field mixed formulation. Insight is gained into the effects and relative importance of the various material parameters upon the response behaviour of the benchmark structure.

The addition of the method presented here for analytical sensitivity computation to finite elements based on a three-field mixed formulation offers a powerful tool for any kind of applications in which finite element response sensitivity analysis results are needed. These applications include structural reliability, structural optimization, structural identification, and finite element model updating. Furthermore, finite element response sensitivity analysis offers insight into structural response behaviour and its sensitivity to modelling parameters.

APPENDIX A

Equation (68) is obtained by differentiating Equation (62) with respect to θ as

$$\overline{\mathbf{E}}\frac{\mathrm{d}\mathbf{e}(\theta)}{\mathrm{d}\theta}-\overline{\mathbf{B}}\frac{\mathrm{d}\mathbf{q}(\theta)}{\mathrm{d}\theta}=\mathbf{0}\ \Rightarrow\ \overline{\mathbf{E}}\frac{\mathrm{d}\mathbf{e}(\theta)}{\mathrm{d}\theta}=\overline{\mathbf{B}}\frac{\mathrm{d}\mathbf{q}(\theta)}{\mathrm{d}\theta} \tag{A1}$$

Pre-multiplying both sides of the second of Equations (A1) by $\overline{\mathbf{D}}_t^{-1}\overline{\mathbf{E}}^{\mathrm{T}}\overline{\overline{\mathbf{D}}}_t^{-1}$, we obtain

$$\overline{\mathbf{D}}_t^{-1}\overline{\mathbf{E}}^{\mathrm{T}}\overline{\overline{\mathbf{D}}}_t^{-1}\overline{\mathbf{E}}\frac{\mathrm{d}\mathbf{e}(\theta)}{\mathrm{d}\theta}=\overline{\mathbf{D}}_t^{-1}\overline{\mathbf{E}}^{\mathrm{T}}\overline{\overline{\mathbf{D}}}_t^{-1}\overline{\mathbf{B}}\frac{\mathrm{d}\mathbf{q}(\theta)}{\mathrm{d}\theta} \tag{A2}$$

Copyright © 2006 John Wiley & Sons, Ltd.

DOI: 10.1002/nme

Using the definition of $\overline{\overline{\mathbf{D}}}_t$ in Equation (70), we have

$$\mathbf{I}_s = \overline{\overline{\mathbf{D}}}_t \overline{\overline{\mathbf{D}}}_t^{-1} = \overline{\mathbf{E}}\overline{\mathbf{D}}_t^{-1}\overline{\mathbf{E}}^{\mathrm{T}}\overline{\overline{\mathbf{D}}}_t^{-1} \tag{A3}$$

where $\mathbf{I}_s$ denotes the unit matrix of dimension $n_s \times n_s$.

Post-multiplying the first and last terms of Equation (A3) by $\overline{\mathbf{E}}$, we have

$$\mathbf{I}_s\overline{\mathbf{E}} = \overline{\mathbf{E}}\overline{\mathbf{D}}_t^{-1}\overline{\mathbf{E}}^{\mathrm{T}}\overline{\overline{\mathbf{D}}}_t^{-1}\overline{\mathbf{E}} \;\Rightarrow\; \overline{\mathbf{E}} = \overline{\mathbf{E}}(\overline{\mathbf{D}}_t^{-1}\overline{\mathbf{E}}^{\mathrm{T}}\overline{\overline{\mathbf{D}}}_t^{-1}\overline{\mathbf{E}}) \tag{A4}$$

from which it can be deduced that

$$\overline{\mathbf{D}}_t^{-1}\overline{\mathbf{E}}^{\mathrm{T}}\overline{\overline{\mathbf{D}}}_t^{-1}\overline{\mathbf{E}} = \mathbf{I}_e \tag{A5}$$

where $\mathbf{I}_e$ denotes the unit matrix of dimension $n_e \times n_e$. Thus, Equation (A2) reduces to Equation (68).

Equation (74) can be derived following a reasoning similar to the one above. Differentiating Equation (63) with respect to θ yields

$$\overline{\mathbf{E}}^{\mathrm{T}}\frac{\mathrm{d}\mathbf{s}(\mathbf{e}(\theta),\theta)}{\mathrm{d}\theta} = \frac{\mathrm{d}\mathbf{a}(\mathbf{e}(\theta),\theta)}{\mathrm{d}\theta} \tag{A6}$$

Pre-multiplying both sides of Equation (A6) by $\overline{\overline{\mathbf{D}}}_t^{-1}\overline{\mathbf{E}}\overline{\mathbf{D}}_t^{-1}$, we obtain

$$\overline{\overline{\mathbf{D}}}_t^{-1}\overline{\mathbf{E}}\overline{\mathbf{D}}_t^{-1}\overline{\mathbf{E}}^{\mathrm{T}}\frac{\mathrm{d}\mathbf{s}(\mathbf{e}(\theta),\theta)}{\mathrm{d}\theta} = \overline{\overline{\mathbf{D}}}_t^{-1}\overline{\mathbf{E}}\overline{\mathbf{D}}_t^{-1}\frac{\mathrm{d}\mathbf{a}(\mathbf{e}(\theta),\theta)}{\mathrm{d}\theta} \tag{A7}$$

Using again Equation (70), we can write

$$\mathbf{I}_s = \overline{\overline{\mathbf{D}}}_t^{-1}\overline{\overline{\mathbf{D}}}_t = \overline{\overline{\mathbf{D}}}_t^{-1}\overline{\mathbf{E}}\overline{\mathbf{D}}_t^{-1}\overline{\mathbf{E}}^{\mathrm{T}} \tag{A8}$$

from which Equation (A7) reduces to Equation (74).

Equations (35) and (43) in Section 3.1 can be derived following the same reasoning used above for Equations (68) and (74), respectively.

APPENDIX B

In this appendix, explicit expressions for the quantities $\mathbf{d}$, $\mathbf{D}$, and $\mathbf{A}_s(\mathbf{X})$ introduced in Section 3.3 are given for three important 2-D frame models: (a) Euler–Bernoulli monolithic beam; (b) Timoshenko monolithic beam; and (c) composite beam with distributed shear connection and Newmark's kinematic assumptions. The extension to 3-D frames is straightforward for the monolithic beams but more complicated for the composite beam with deformable shear connection [27].

(a) *Euler–Bernoulli monolithic beam* (Figure B1):

$$\mathbf{A}_s(x, y, \theta) = [1 \;\; -y] \tag{B1}$$

$$\boldsymbol{\varepsilon}(\mathbf{X}, \theta) \equiv \varepsilon_x(x, y, \theta), \quad \boldsymbol{\sigma}(\mathbf{X}, \theta) \equiv \sigma_x(x, y, \theta) \tag{B2}$$

Copyright © 2006 John Wiley & Sons, Ltd.

DOI: 10.1002/nme

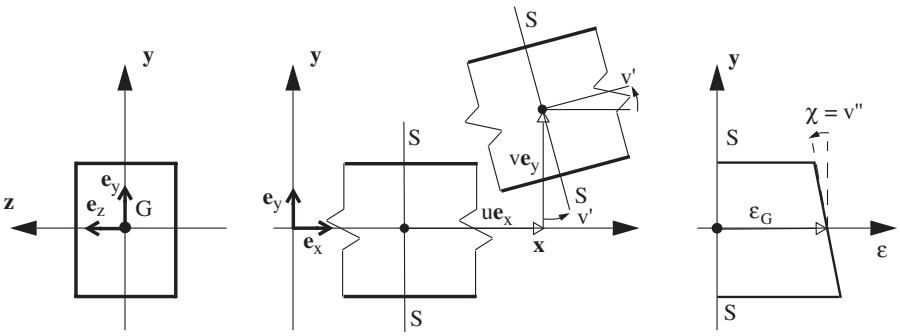

Figure B1. Kinematics of 2-D monolithic Euler–Bernoulli beam model.

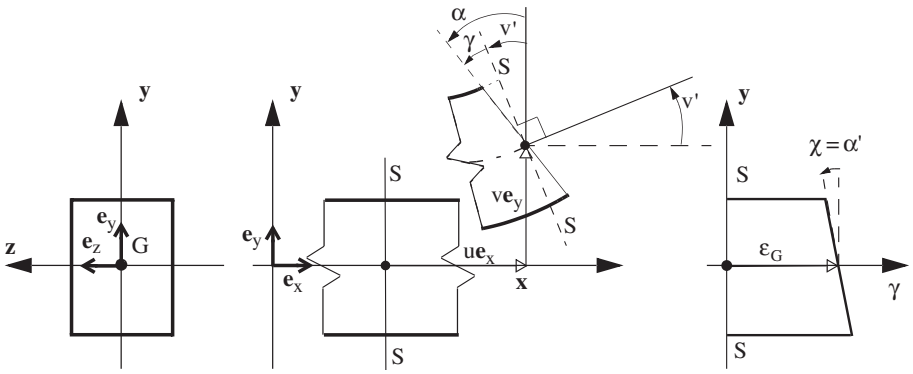

Figure B2. Kinematics of 2-D monolithic Timoshenko beam model.

$$\mathbf{d}(x, \theta) = \begin{bmatrix} \varepsilon_G(x, \theta) \\ \chi(x, \theta) \end{bmatrix} \tag{B3}$$

$$\mathbf{D}(x, \theta) = \begin{bmatrix} N(x, \theta) \\ M(x, \theta) \end{bmatrix} \tag{B4}$$

(b) *Timoshenko monolithic beam* (Figure B2):

$$\mathbf{A}_s(x, y, \theta) = \begin{bmatrix} 1 & -y & 0 \\ 0 & 0 & 1 \end{bmatrix} \tag{B5}$$

$$\boldsymbol{\varepsilon}(\mathbf{X}, \theta) \equiv \begin{bmatrix} \varepsilon_x(x, y, \theta) \\ \gamma_{xy}(x, y, \theta) \end{bmatrix}, \quad \boldsymbol{\sigma}(\mathbf{X}, \theta) \equiv \begin{bmatrix} \sigma_x(x, y, \theta) \\ \tau_{xy}(x, y, \theta) \end{bmatrix} \tag{B6}$$

Copyright © 2006 John Wiley & Sons, Ltd.

DOI: 10.1002/nme

$$\mathbf{d}(x,\theta)=\begin{bmatrix}\varepsilon_G(x,\theta)\\ \chi(x,\theta)\\ \gamma(x,\theta)\end{bmatrix} \tag{B7}$$

$$\mathbf{D}(x,\theta)=\begin{bmatrix}N(x,\theta)\\ M(x,\theta)\\ V(x,\theta)\end{bmatrix} \tag{B8}$$

(c) *Newmark composite beam* (Figure 1):

$$\mathbf{A}_s(x,y,\theta)=\begin{bmatrix}1 & 0 & (y_1-y) & 0\\ 0 & 1 & (y_2-y) & 0\\ 0 & 0 & 0 & 1\end{bmatrix} \tag{B9}$$

$$\boldsymbol{\varepsilon}(\mathbf{X},\theta)\equiv\begin{bmatrix}\varepsilon_{x1}(x,y,\theta)\\ \varepsilon_{x2}(x,y,\theta)\\ \delta_s(x,\theta)\end{bmatrix}\quad \sigma(\mathbf{X},\theta)\equiv\begin{bmatrix}\sigma_{x1}(x,y,\theta)\\ \sigma_{x2}(x,y,\theta)\\ f_s(x,\theta)/A(x)\end{bmatrix} \tag{B10}$$

$$\mathbf{d}(x,\theta)=\begin{bmatrix}\varepsilon_{x1}(x,\theta)\\ \varepsilon_{x2}(x,\theta)\\ \chi(x,\theta)\\ \delta_s(x,\theta)\end{bmatrix} \tag{B11}$$

$$\mathbf{D}(x,\theta)=\begin{bmatrix}N_1(x,\theta)\\ N_2(x,\theta)\\ M_{12}(x,\theta)\\ f_s(x,\theta)\end{bmatrix} \tag{B12}$$

ACKNOWLEDGEMENTS

Support of this research by the National Science Foundation under Grant No. CMS-0010112 and by the Pacific Earthquake Engineering Research (PEER) Center through the Earthquake Engineering Research Centers Program of the National Science Foundation under Award No. EEC-9701568 are gratefully acknowledged. Any opinions, findings, and conclusions or recommendations expressed in this material are those of the authors and do not necessarily reflect those of the sponsors.

Copyright © 2006 John Wiley & Sons, Ltd.

DOI: 10.1002/nme

REFERENCES

1. Ditlevsen O, Madsen HO. *Structural Reliability Methods*. Wiley: New York, 1996.
2. Kleiber M, Antunez H, Hien TD, Kowalczyk P. *Parameter Sensitivity in Nonlinear Mechanics*: *Theory and Finite Element Computations*. Wiley: New York, 1997.
3. Zhang Y, Der Kiureghian A. Dynamic response sensitivity of inelastic structures. *Computer Methods in Applied Mechanics and Engineering* 1993; **108**(1–2):23–36.
4. Conte JP. Finite element response sensitivity analysis in earthquake engineering. *Earthquake Engineering Frontiers in the New Millennium*. Spencer & Hu/Swets & Zeitlinger: Lisse, The Netherlands, 2001; 395–401.
5. Conte JP, Vijalapura PK, Meghella M. Consistent finite-element response sensitivity analysis. *Journal of Engineering Mechanics* (ASCE) 2003; **129**(12):1380–1393.
6. Conte JP, Barbato M, Spacone E. Finite element response sensitivity analysis using force-based frame models. *International Journal for Numerical Methods in Engineering* 2004; **59**(13):1781–1820.
7. Scott MH, Franchin P, Fenves GL, Filippou FC. Response sensitivity for nonlinear beam-column elements. *Journal of Structural Engineering* (ASCE) 2004; **130**(9):1281–1288.
8. Barbato M, Conte JP. Finite element response sensitivity analysis: a comparison between force-based and displacement-based frame element models. *Computer Methods in Applied Mechanics and Engineering* 2005; **194**(12–16):1479–1512.
9. Pian THH. Derivation of element stiffness matrices by assumed stress distribution. *AIAA Journal* 1964; **2**(7):1333–1336.
10. Chien WZ. Method of high-order Lagrange multiplier and generalized variational principles of elasticity with more general forms of functionals. *Applied Mathematics and Mechanics* 1983; **4**(2):137–150.
11. Washizu K. *Variational Methods in Elasticity and Plasticity*. Pergamon Press: Oxford, 1975.
12. Malkus DS, Hughes TJR. Mixed finite element methods-reduced and selective integration techniques: a unification of concepts. *Computer Methods in Applied Mechanics and Engineering* 1978; **15**(1):63–81.
13. Noor AK. Multifield (mixed and hybrid) finite element models. *State-of-the-Art Surveys on Finite Element Technology*, Noor AK, Pilkey WD (eds). ASME: New York, 1983; 127–156.
14. Belytschko T, Liu WK, Moran B. *Nonlinear Finite Elements for Continua and Structures*. Wiley: New York, 2000.
15. Fraeijs De Veubeke BM. Displacement and equilibrium models in the finite element method. *Stress Analysis*, Zienkiewicz OC, Hollister GS (eds). Wiley: London, 1965; 145–196; Reprinted in: *International Journal for Numerical Methods in Engineering* 2001; **52**(3):287–342.
16. Stolarski H, Belytschko T. Limitation principles for mixed finite elements based on the Hu–Washizu variational formulation. *Computer Methods in Applied Mechanics and Engineering* 1987; **60**(2):195–216.
17. Mota A, Abel JF. On mixed finite element formulation and stress recovery techniques. *International Journal for Numerical Methods in Engineering* 2000; **47**(1–3):191–204.
18. Pandey PC, Bakshi P. Analytical response sensitivity computation using hybrid finite elements. *Computers and Structures* 1999; **71**(5):525–534.
19. Spacone E, Ciampi V, Filippou FC. Mixed formulation of nonlinear beam finite element. *Computers and Structures* 1995; **58**(1):71–83.
20. Spacone E, Filippou FC, Taucer FF. Fibre beam-column element for nonlinear analysis of R/C frames. Part I: Formulation. *Earthquake Engineering and Structural Dynamics* 1996; **25**(7):711–725.
21. Taylor RL, Filippou FC, Saritas A, Auricchio F. A mixed element method for beam and frame problems. *Computational Mechanics* 2003; **31**(1–2):192–103.
22. Ayoub A, Filippou FC. Mixed formulation of nonlinear steel–concrete composite beam element. *Journal of Structural Engineering* (ASCE) 2000; **126**(3):371–381.
23. Dall'Asta A, Zona A. Three-field mixed formulation for the non-linear analysis of composite beams with deformable shear connection. *Finite Elements in Analysis and Design* 2004; **40**(4):425–448.
24. Newmark NM. A method of computation for structural dynamics. *Journal of the Engineering Mechanics Division* (ASCE) 1959; **85**:67–94.
25. Spacone E, El-Tawil S. Nonlinear analysis of steel–concrete composite structures: state of the art. *Journal of Structural Engineering* (ASCE) 2004; **130**(2):159–168.
26. Oehlers DJ, Bradford MA. *Elementary Behaviour of Composite Steel and Concrete Structural Members*. Butterworth-Heinemann: Oxford, 2000.
27. Dall'Asta A. Composite beams with weak shear connection. *International Journal of Solids and Structures* 2001; **38**(32–33):5605–5624.

Copyright © 2006 John Wiley & Sons, Ltd.

DOI: 10.1002/nme

28. Newmark NM, Siess CP, Viest IM. Tests and analysis of composite beams with incomplete interaction. *Proceedings, Society for Experimental Stress Analysis* 1951; **9**(1):75–92.
29. Dall'Asta A, Zona A. Non-linear analysis of composite beams by a displacement approach. *Computers and Structures* 2002; **80**(27–30):2217–2228.
30. Dall'Asta A, Zona A. Slip locking in finite elements for composite beams with deformable shear connection. *Finite Elements in Analysis and Design* 2004; **40**(13–14):1907–1930.
31. Dall'Asta A, Zona A. Comparison and validation of displacement and mixed elements for the non-linear analysis of continuous composite beams. *Computers and Structures* 2004; **82**(23–26):2117–2130.
32. Zona A, Barbato M, Conte JP. Finite element response sensitivity analysis of steel–concrete composite beams with deformable shear connection. *Journal of Engineering Mechanics* (ASCE) 2005; **131**(11):1126–1139.
33. Filippou FC, Constantinides M. FEDEASLab getting started guide and simulation examples. *Technical Report NEESgrid-2004-22*, 31 August 2004. http://fedeaslab.berkeley.edu/
34. Matlab—high performance numeric computation and visualization software. *User's Guide*. The MathWorks Inc., Natick, MA, 1997.
35. Franchin P. Reliability of uncertain inelastic structures under earthquake excitation. *Journal of Engineering Mechanics* (ASCE) 2003; **130**(2):180–191.
36. Loma Prieta 1989 Accelerograms. *PEER Strong Motion Database*. http://peer.berkeley.edu/smcat/
37. Balan TA, Spacone E, Kwon M. A 3D hypoplastic model for cyclic analysis of concrete structures. *Engineering Structures* 2001; **23**(4):333–342.
38. Balan TA, Filippou FC, Popov EP. Constitutive model for 3D cyclic analysis of concrete structures. *Journal of Engineering Mechanics* (ASCE) 1997; **123**(2):143–153.
39. Ollgaard JG, Slutter RG, Fisher JW. Shear strength of stud connectors in lightweight and normal weight concrete. *Engineering Journal* (AISC) 1971; **2Q**:55–64.
40. Eligenhausen R, Popov EP, Bertero VV. Local bond stress–slip relationships of deformed bars under generalized excitations. *Report No. 83/23*, EERC Earthquake Engineering Research Center, University of California, Berkeley, CA, 1983.
41. Zona A, Barbato M, Conte JP. Finite element response sensitivity analysis of steel–concrete composite structures. *Report SSRP-04/02*, Department of Structural Engineering, University of California, San Diego, CA, 2004.
42. Haftka RT, Gurdal Z. *Elements of Structural Optimization* (3rd edn). Kluwer Academic Publishers: Dordrecht, 1993.
43. Chopra AK. *Dynamics of Structures*: *Theory and Applications to Earthquake Engineering* (2nd edn). Prentice-Hall: Englewood Cliffs, NJ, 2001.

Copyright © 2006 John Wiley & Sons, Ltd.

DOI: 10.1002/nme